An Introduction to Plasma and Feature Scale Modeling in the Semiconductor Industry

Shahid Rauf
Managing Director, Plasma Products Modeling
Applied Materials, Inc., Santa Clara, CA

PPPL Summer School
Princeton, NJ, USA
July 28 – August 1, 2025

Agenda

- Plasmas in the Semiconductor Industry
- Plasma and Feature Scale Modeling
- Modeling Examples
  - Global models
  - Plasma uniformity
  - Plasma breakdown
  - Feature scale modeling
  - Plasma – surface interaction
- Conclusions

Plasmas and the Semiconductor Industry

- It's hard to picture life in 2025 without microelectronics—they're everywhere!
- Low-temperature plasmas are a key technology used for microelectronics manufacturing:
  - Etching
  - Deposition
  - Cleaning and surface preparation
  - Material modification

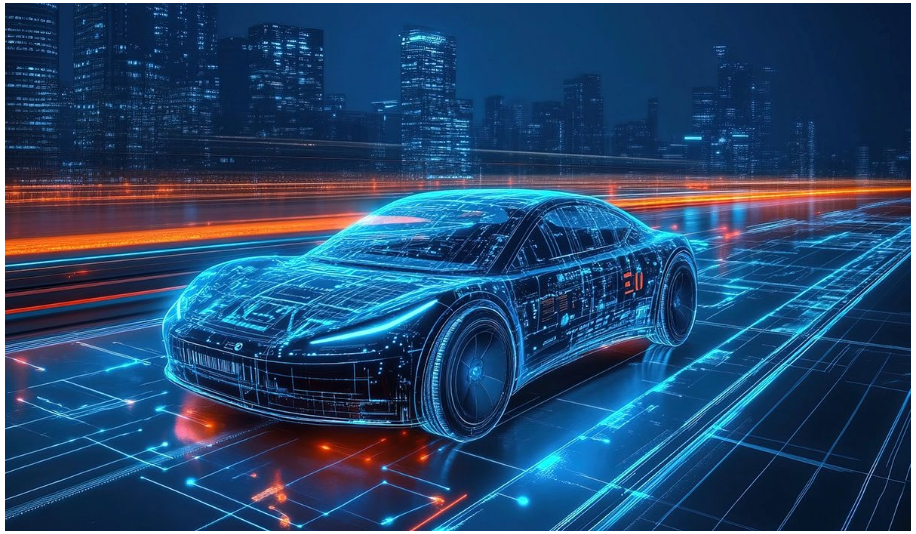

APPLIED MATERIALS®

Plasmas and Microelectronics Fabrication

- Microelectronics fabrication requires 100s of processing steps, many plasma based.

Plasma Enhanced Deposition

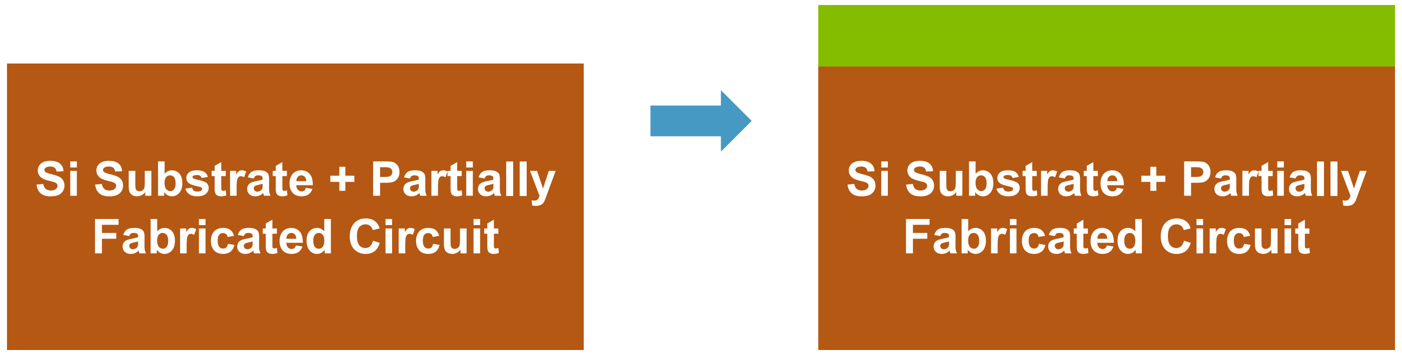

Plasmas and Microelectronics Fabrication

- Microelectronics fabrication requires 100s of processing steps, many plasma based.

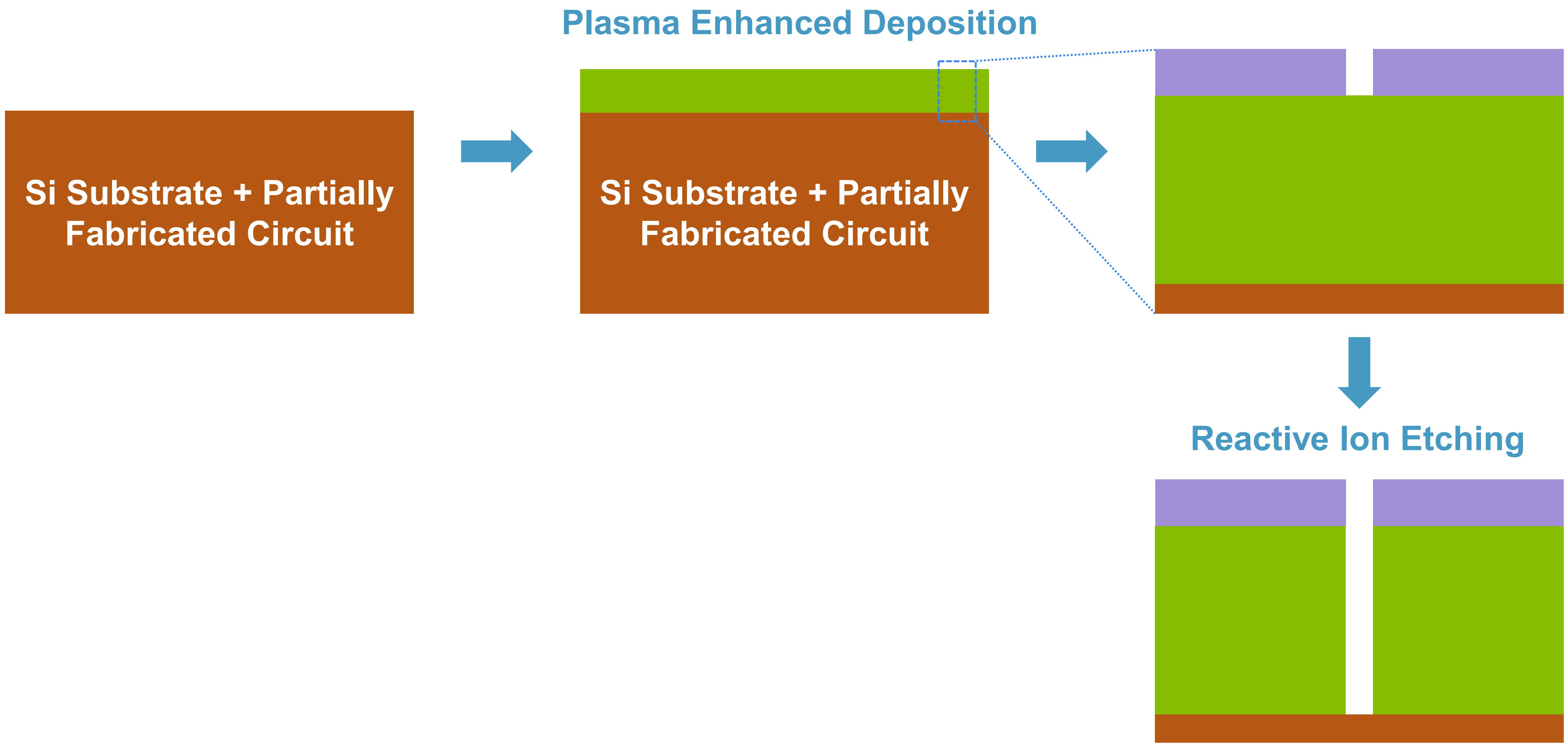

Plasmas and Microelectronics Fabrication

- Microelectronics fabrication requires 100s of processing steps, many plasma based.

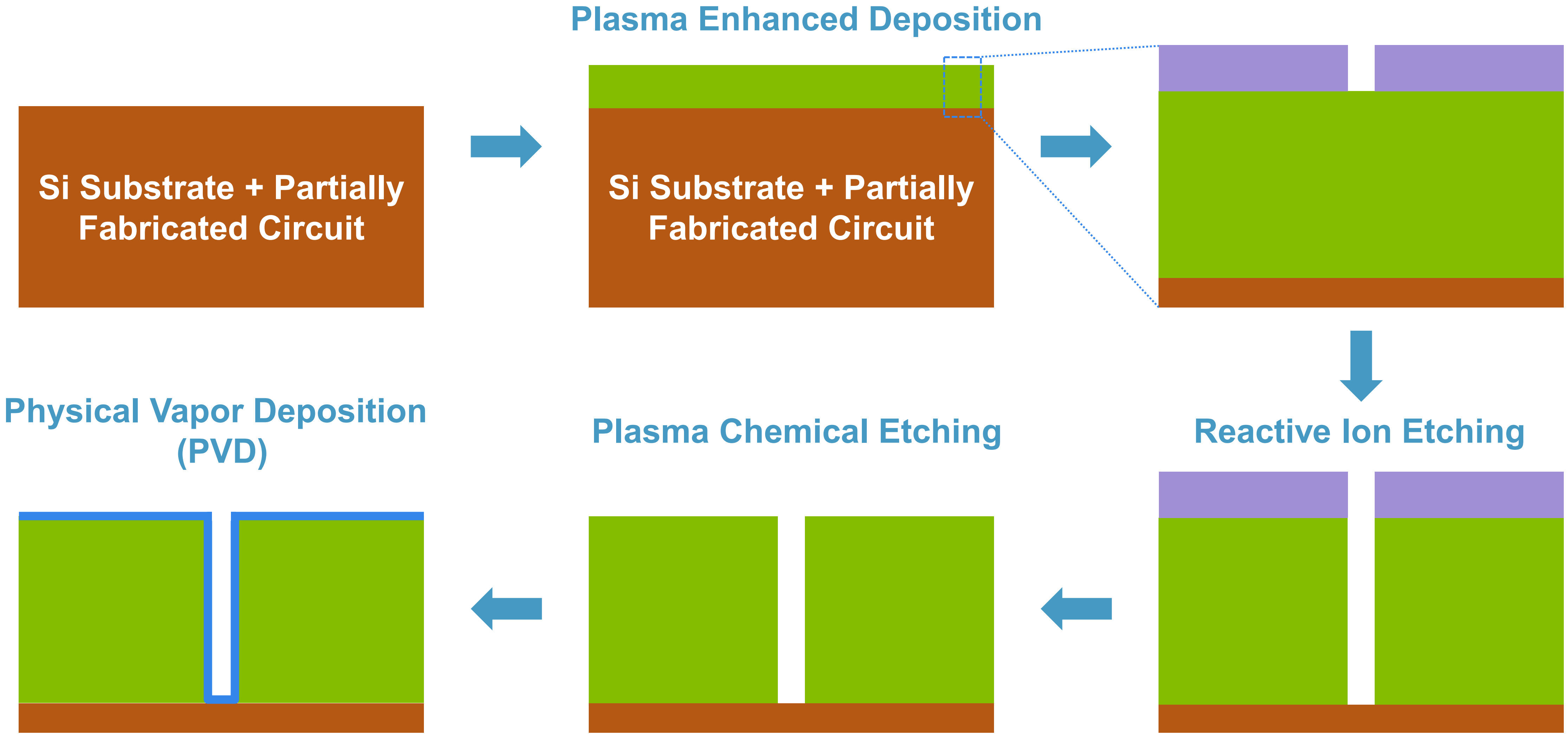

Typical Plasma Sources in Semiconductor Industry

- Many plasma sources are used in the semiconductor industry including the following:

Capacitively Coupled Plasma

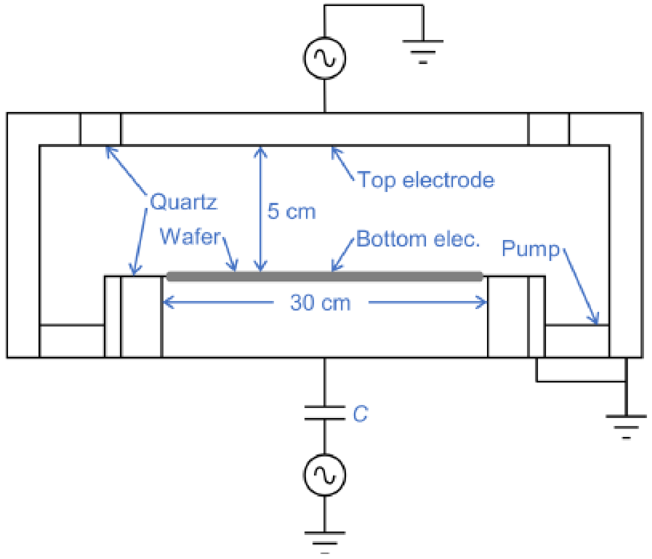

Inductively Coupled Plasma

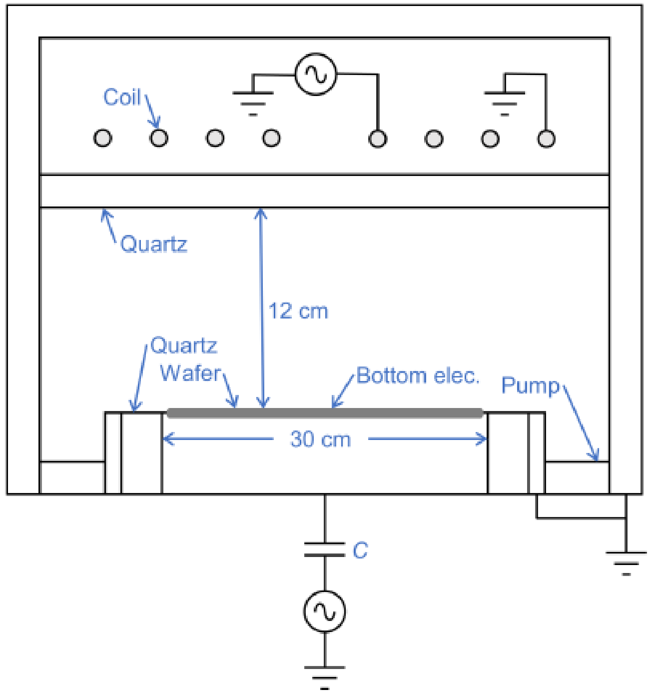

Magnetron Based PVD Source

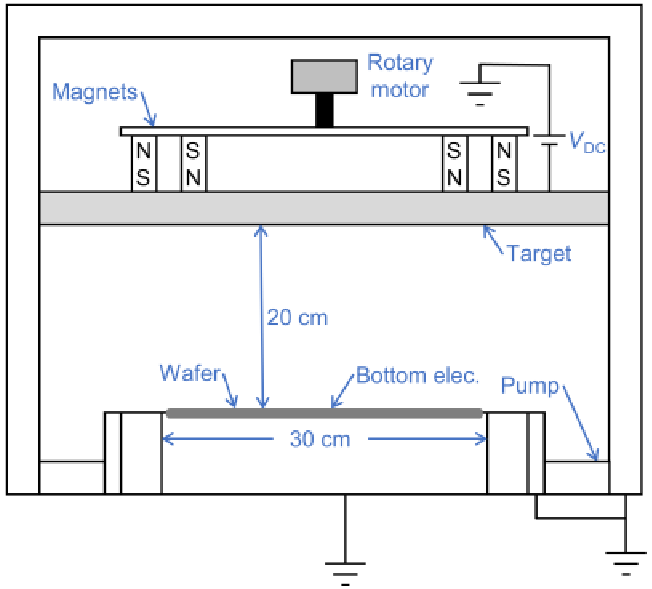

References

Rauf *et al.*, J. Micro/Nanopattern. Mater. Metrol. 22, 041503 (2023)

Plasma and Feature Scale Modeling

Plasma and Feature Scale Modeling Ecosystem in Semiconductor Industry

- Semiconductor industry is one of the largest employers of plasma modeling engineers.

Suppliers

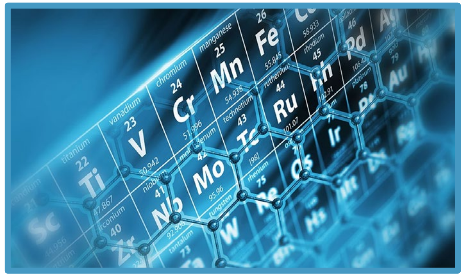

e.g., Air Products, AE

Equipment Vendors

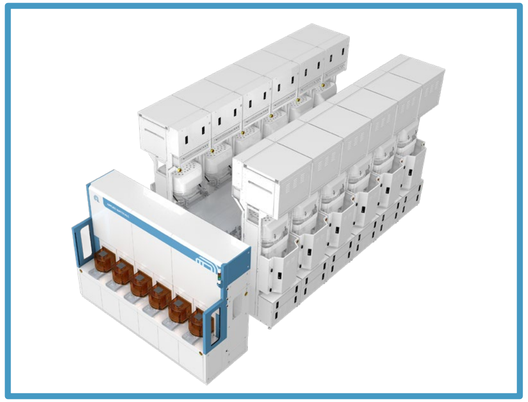

e.g., AMAT, Lam, TEL

Software Vendors

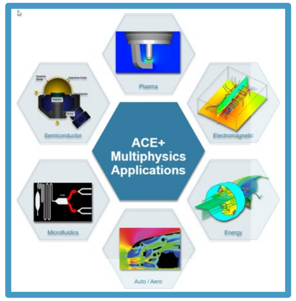

e.g., Synopsys, Comsol

Microelectronics Manufacturers

e.g., TSMC, Sony, Intel

APPLIED MATERIALS

Plasma and Feature Scale Modeling Toolbox

- Plasma modeling engineers in industry:
  - Actively participate in R&D, product design, and customer communication
  - Work on a diverse set of technically challenging problems
  - **Need strong foundation in plasma physics and plasma – surface interactions to be successful**

Plasma and Feature Scale Modeling Toolbox

- Plasma modeling engineers in industry:
  - Actively participate in R&D, product design, and customer communication
  - Work on a diverse set of technically challenging problems
  - **Need strong foundation in plasma physics and plasma – surface interactions to be successful**
  - Use a variety of specialized software tools

Plasma Modeling	Feature Scale Modeling	Atomistic Modeling
Global Fluid and hybrid Kinetic	String and level-set Monte Carlo	Molecular dynamics Quantum chemistry

General Tools

- Python
- Excel
- Fortran / C++

References

Rauf *et al.*, J. Micro/Nanopattern. Mater. Metrol. 22, 041503 (2023)
Kuboi, J. Micro/Nanopattern. Mater. Metrol. 22, 041502 (2023)
Alves *et al.*, Plasma Sources Sci. Technol. 27, 023002 (2018)

Plasma Modeling – Global Models

- Global or 0D models use judicious assumptions to develop simple models for plasma systems:
  - Spatial shape of plasma, $g_i(\boldsymbol{x})$
  - Power deposition mechanism
  - Electron energy distribution function (EEDF) or Boltzmann equation
- Global models are fast and can afford to model detailed chemistries.
- Plasma physics and chemistry expertise is critical to develop good global models.
- Available global models include:
  - Quantemol Global Model (Quantemol-DB)
  - ZDPlasKin

Well-Stirred Reactor

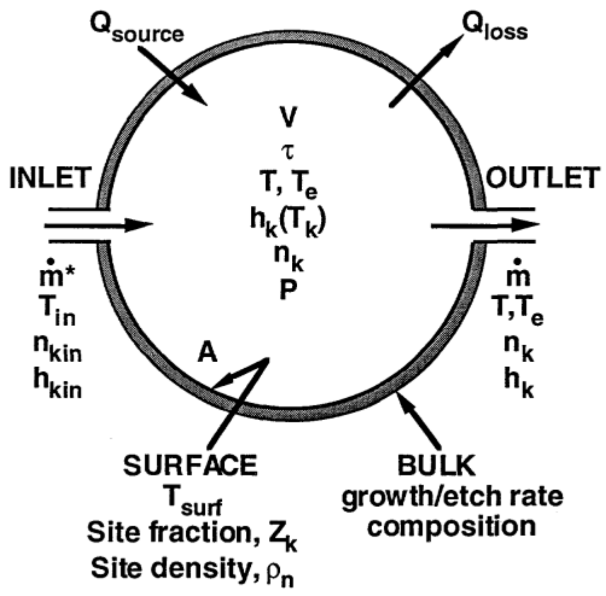

References

Lieberman and Lichtenberg, Principles of Plasma Discharges and Materials Processing (2025)
Chabert and Braithwaite, Physics of Radio-Frequency Plasmas (2011)
Meeks *et al.*, AURORA, Sand-96-8218 (1996)

Plasma Modeling – Fluid and Hybrid Models

- Fluid plasma models are the most widely used in industry.
- Fluid models are relatively fast, available in 1, 2, and 3-D, most mature and well-studied, and flexible with many physics options.
- Hybrid models add kinetic treatment of athermal electrons and ions in fluid models.
- Available fluid and hybrid plasma models include:
  - Quantemol-VT (HPEM)
  - CFD-ACE+ (ACE+ - Applied Materials)
  - COMSOL Plasma Module
  - Vizglow (OverViz - Lam Research)

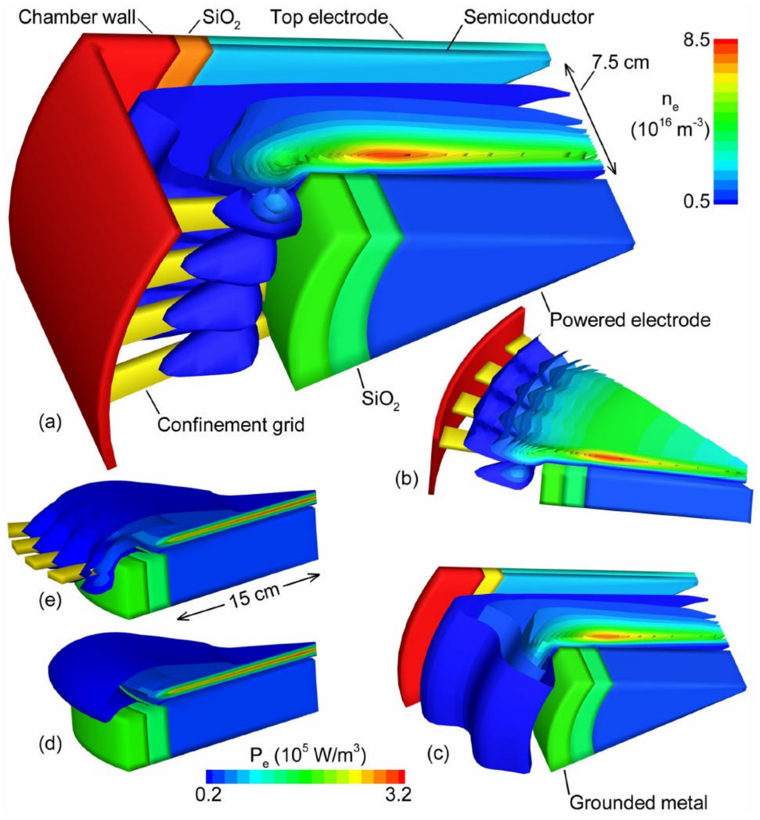

Fig. 1. (a) Electron density in the CCP reactor with the confinement grid, (b) another view of electron density in the reactor with confinement grid, (c) electron density in the system without the confinement grid, (d) electron power deposition without the confinement grid, and (e) electron power deposition in the reactor with confinement grid. Simulations are for 100 mtorr gas pressure in Ar, 500 W applied from bottom electrode at 60 MHz, and 7.5 cm interelectrode spacing. Only a 40° slice is shown for clarity.

Kenney, Rauf, and Collins, IEEE Trans. Plasma Sci. 36, 1364 (2008)

References

Rauf *et al.*, J. Micro/Nanopattern. Mater. Metrol. 22, 041503 (2023)
Kushner, J. Phys. D: Appl. Phys. 42, 194013 (2009)
Alves *et al.*, Plasma Sources Sci. Technol. 27, 023002 (2018)

Plasma Modeling – Kinetic Modeling

- Kinetic plasma models become essential for simulating:
  - low pressure and magnetized plasmas
  - discharges where kinetic phenomena are important
- Particle-in-Cell with Monte Carlo Collisions (PIC/MCC) is the most widely used kinetic plasma modeling technique.
- PIC simulations are usually slow, and PIC codes are often physics-focused with limited bells-and-whistles for industrial use.
- Available PIC modeling codes include
  - EDIPIC (Princeton Plasma Physics Lab)
  - WarpX (Lawrence Berkeley Lab)
  - VSimPlasma (Tech-X)

Effect of Magnetic Field on Electron Density

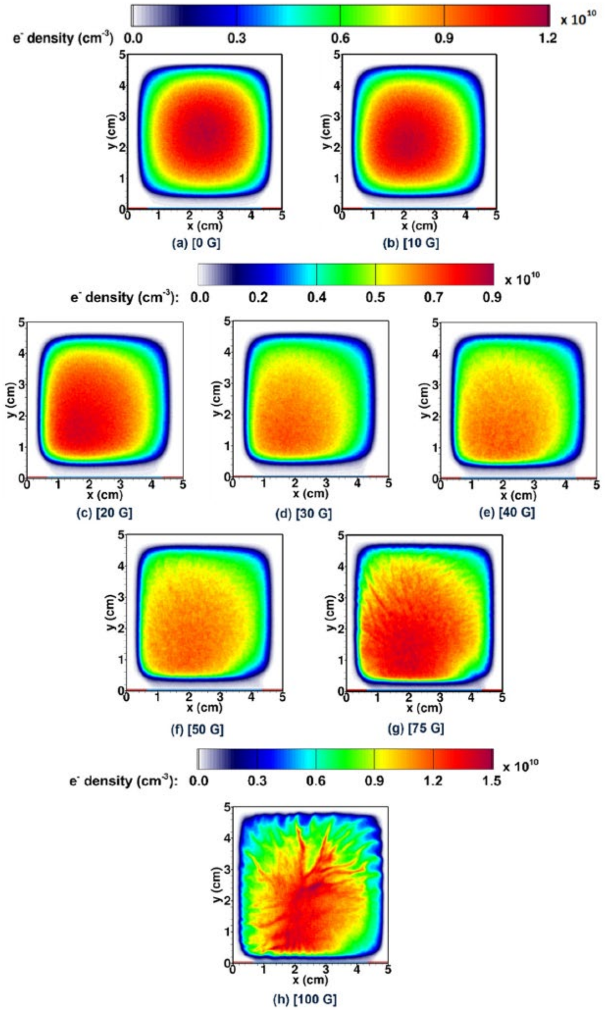

Ganta *et al.*, Phys. Plasmas 31, 102107 (2024)

References

Birdsall and Langdon, Plasma Physics via Computer Simulation, 1991

Feature Scale Modeling – Monte Carlo

- Monte Carlo methods are commonly used to model plasma interaction with surfaces.
- These models approximate the material as a 2 or 3-D array of voxels representing atomic clusters.
- Plasma species with given fluxes and energy + angular distributions are introduced from the top.
- The reaction mechanism dictates the interaction of ions and neutrals from the plasma with the surface.
- Available Monte Carlo feature scale model include:
  - MCFPM (University of Michigan)
  - Pagasus FPSM2D

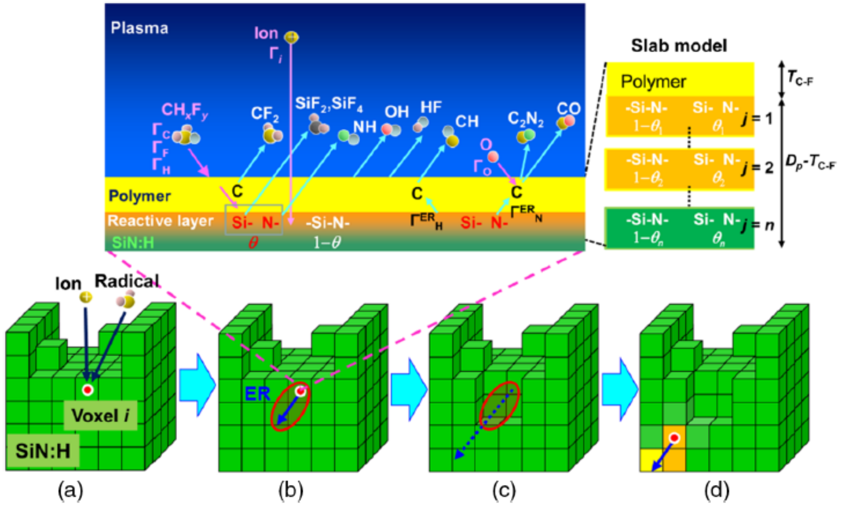

Fig. 19 Schematic drawing of calculation procedure through (a), (b), (c), and (d) for 3D voxel-slab model.[69]

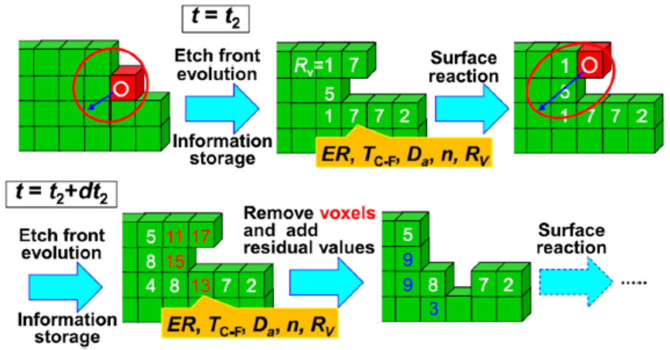

Fig. 20 Schematic drawing of etch front evolution for 3D voxel-slab model. The red circle at the red voxel represents an etched region related to the derive ER and red values in voxels exceed the threshold to be removed.[69]

References

Kuboi, J. Micro/Nanopattern. Mater. Metrol. 22, 041502 (2023)

Atomistic Modeling – Molecular Dynamics

- Molecular dynamics (MD) is a widely used technique in material science and quantum chemistry.
- MD combines potentials (derived from ab-initio computations) with classical physics to simulate the dynamics of large cluster of atoms.
- MD is used by the low-temperature plasma community to study plasma etch processes.
- Availability and accuracy of potentials are important issues in MD modeling.
- Many MD models are available (MD Software – Wikipedia) including:
  - LAMMPS (Sandia National Lab)

MD Simulation of SiO_2/Si Etch

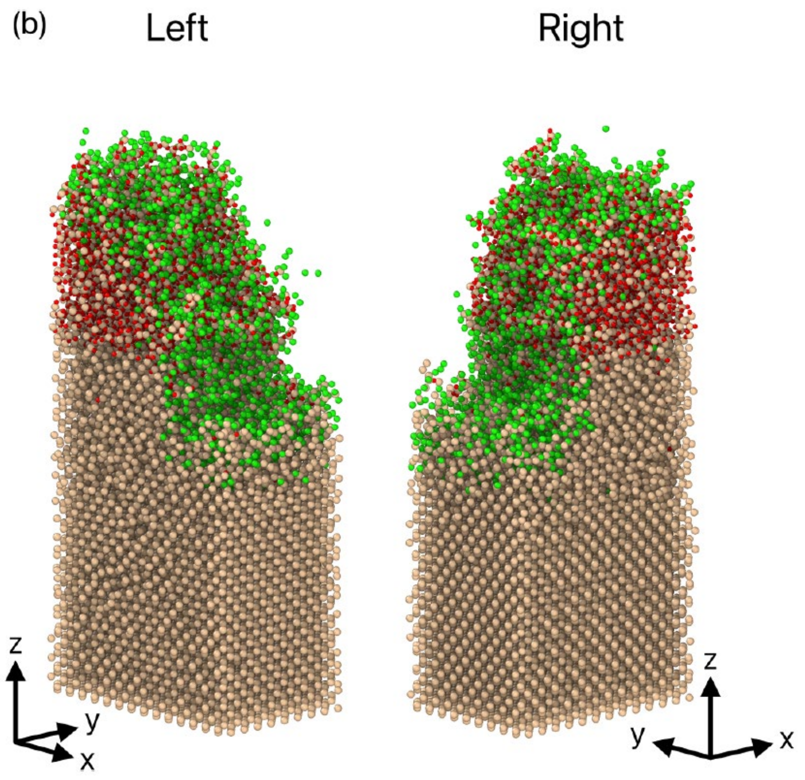

Mauchamp and Hamaguchi, J. Vac. Sci. Technol. A 40, 053004 (2022)

References

Frenkel and Smit, Understanding Molecular Simulation (2001)
Griebel, Knapek, and Zumbusch, Numerical Simulation in Molecular Dynamics (2010)
Mubin and Li, Extending and Modifying LAMMPS (2021)

Modeling Examples

Ho – SiO_2 Etch in C_2F_6 Plasma – Model

- Ho *et al.* developed a 0D model for SiO_2 etch in C_2F_6 plasma using Aurora.
- C_2F_6 mechanism: 28 species and 132 reactions.
- SiO_2 etch mechanism: 6 species and 85 reactions.
- Assumptions: spatially uniform, Maxwellian electrons.
- Tested the model using experimental data from 3 ICP reactors.

ICP Reactors

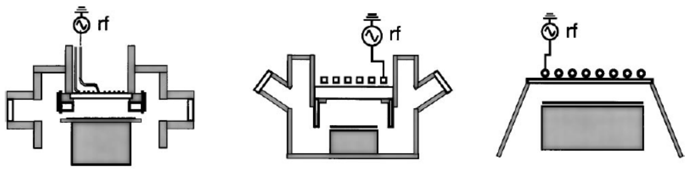

Mechanism – C_2F_6 Plasma and SiO_2 Etch

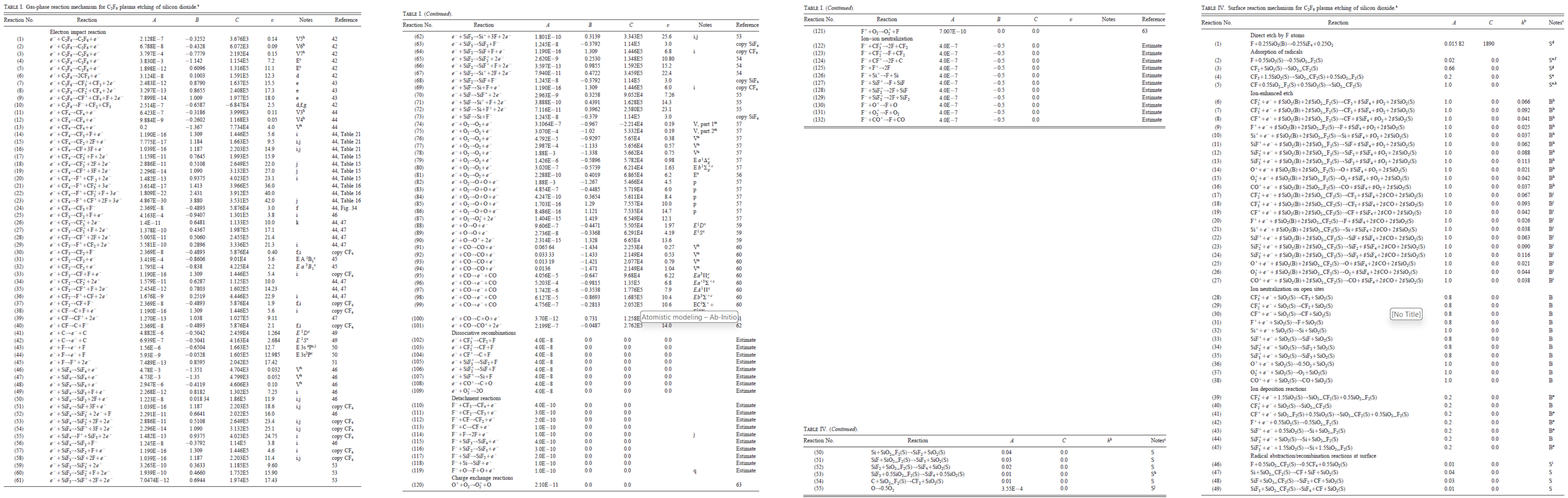
TABLE I. Gas-phase reaction mechanism for C_2F_6 plasma etching of silicon dioxide.
TABLE I. (Continued).
TABLE I. (Continued).
TABLE IV. Surface reaction mechanism for C_2F_6 plasma etching of silicon dioxide.
TABLE IV. (Continued).

Ho *et al.*, J. Vac. Sci. Technol. A 19, 2344 (2001)

Ho – SiO_2 Etch in C_2F_6 Plasma – Comparison to Experiments

- Ho *et al.* compared their 0D modeling results to a wide variety of experimental data:
  - SiO_2 etch rate over a range of conditions in 2 chambers
  - F, SiF, and CF_x radical densities
  - Electron density

Etch Rate – Model vs. Experiment

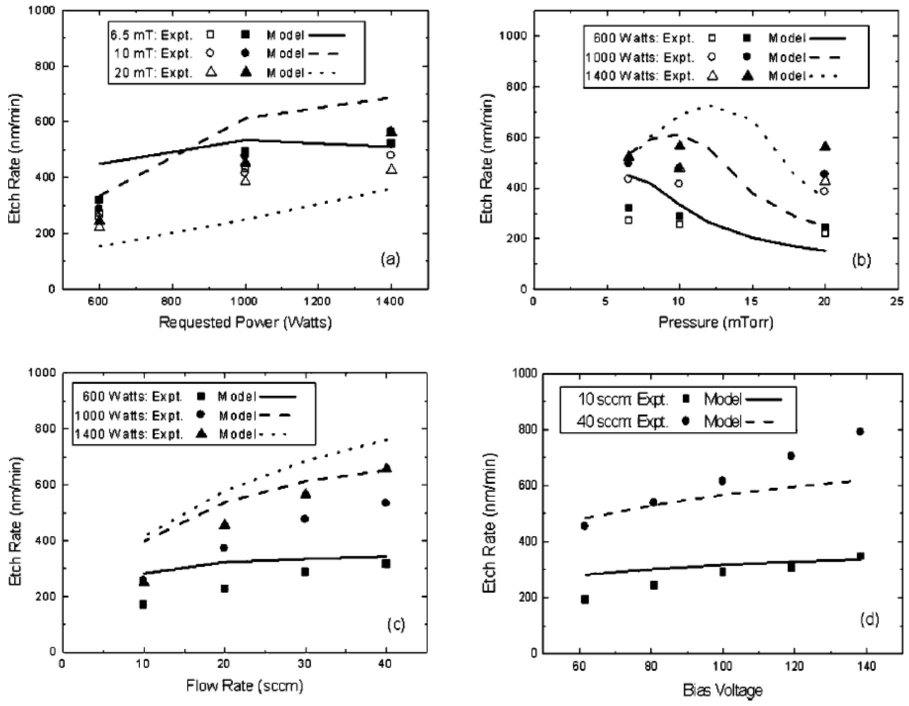

F Density – Model vs. Experiment

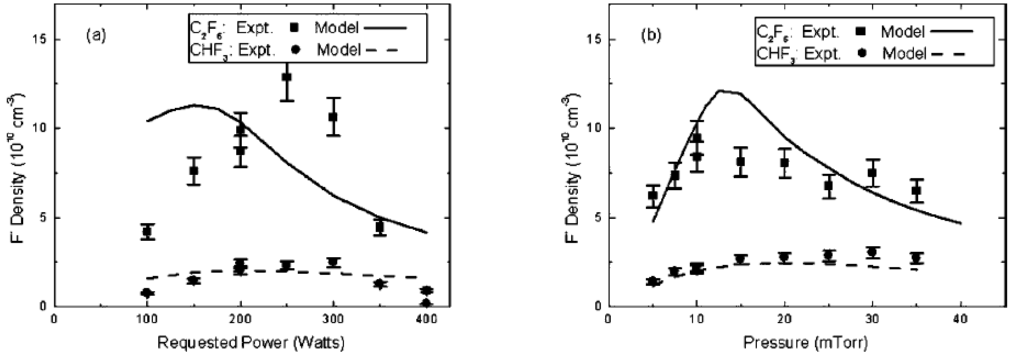

SiO_2 Etch Mechanism – Reactor III

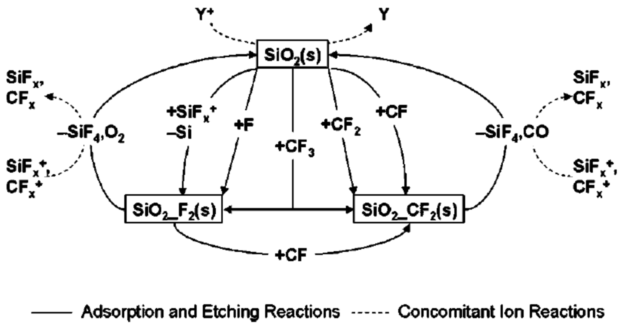

Ho *et al.*, J. Vac. Sci. Technol. A 19, 2344 (2001)

Tao – Ionized PVD of TiN – Model

- Tao, Mao, and Hopwood developed a global model for TiN ionized physical vapor deposition (IPVD).
- Model targeted towards 1 experimental system.
- Plasma chemistry is relatively simple with important Ar, N and Ti species included.
- Assumptions: volume averaged densities, sputtered Ti fully thermalized, TiN forms on surface.

TiN IPVD Reactor

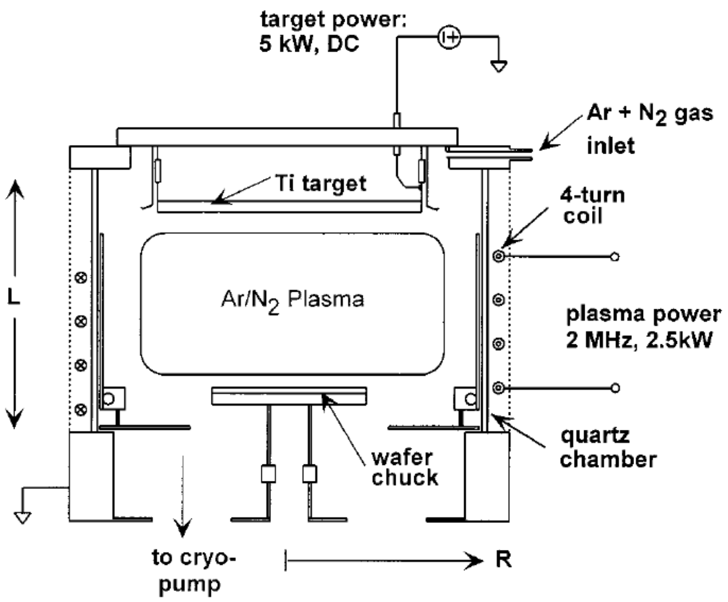

Ti/Ar/N_2 Plasma Chemistry

Reaction	Rate constants	Reference
$N + e^- \rightarrow N^+ + 2e^-$	$K_1 = 3.84 \times 10^{-9} (T_e)^{0.92} \exp(-12.1/T_e)$ $cm^3\ s^{-1}$	a
$N_2 + e^- \rightarrow N_2^+ + 2e^-$	$K_2 = 1.95 \times 10^{-9} (T_e)^{1.13} \exp(-14.4/T_e)$ $cm^3\ s^{-1}$	b
$N_2 + e^- \rightarrow 2N + e^-$	$K_3 = 6.15 \times 10^{-9} (T_e)^{0.81} \exp(-12.8/T_e)$ $cm^3\ s^{-1}$	c
$N^+ + N_2 \rightarrow N_2^+ + N$	$K_5 = 2.0 \times 10^{-11}$ $cm^3\ s^{-1}$	d
$N + N_2^+ \rightarrow N^+ + N_2$	$K_6 = 1.0 \times 10^{-11}$ $cm^3\ s^{-1}$	e
$N_2^* + N \rightarrow N + N_2$	$K_7 = 4.0 \times 10^{-11}$ $cm^3\ s^{-1}$	f
$N_2^* + N_2 \rightarrow 2N_2$	$K_8 = 3.5 \times 10^{-12}$ $cm^3\ s^{-1}$	g
$N_2 + e^- \rightarrow N_2^* + e^-$	$K_9 = 5.81 \times 10^{-9} \exp(-7.57/T_e)$ $cm^3\ s^{-1}$	h
$N_2^* \rightarrow N_2 + h\nu$	$\tau_{h\nu} = 2.3 \times 10^{-4}$ s	g
$N(wall) \rightarrow \frac{1}{2} N_2(g)$	$\tau_N^{-1} = D_N / \Lambda_N^2$ s^{-1}	i
$Ar^+ + N_2 \rightarrow N_2^+ + Ar$	$K_{10} = 1.2 \times 10^{-11}$ $cm^3\ s^{-1}$	j
$Ar + e^- \rightarrow Ar^* + e^-$	$K_{11} = 2.2 \times 10^{-8} \exp(-12.4/T_e)$ $cm^3\ s^{-1}$	k
$Ar^* + e^- \rightarrow Ar^+ + 2e^-$	$K_{12} = 2.1 \times 10^{-7} \exp(-5.3/T_e)$ $cm^3\ s^{-1}$	l
$Ar + e^- \rightarrow Ar^+ + 2e^-$	$K_{13} = 1.23 \times 10^{-7} \exp(-18.68/T_e)$ $cm^3\ s^{-1}$	m
$Ti + e^- \rightarrow Ti^+ + 2e^-$	$K_{14} = 2.34 \times 10^{-7} \exp(-7.25/T_e)$ $cm^3\ s^{-1}$	n
$Ti + Ar^* \rightarrow Ti^+ + Ar + e^-$	$K_{15} = \sigma_{Ti} \cdot v_{th\_Ti}$ $cm^3\ s^{-1}$	o

Tao, Mao, and Hopwood, J. Appl. Phys. 91, 4040 (2002)

Tao – Ionized PVD of TiN – Comparison to Experiments

- Tao *et al.* tested their model using experimental measurements in the IPVD chamber.
- Decent model – experiment agreement achieved.
- Assumed different sticking coefficient for N at low and high N_2 flows to explain experimental observation.

TiN IPVD Model – Experiment Comparison

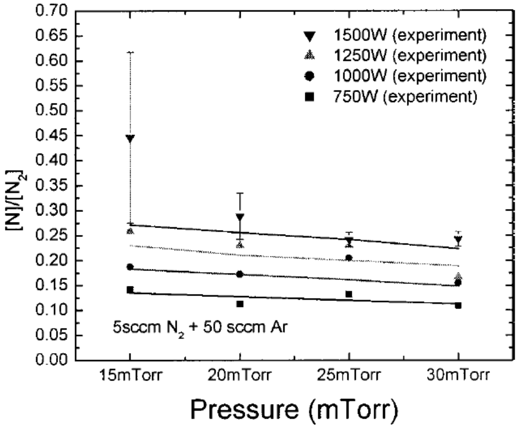

FIG. 3. Comparison of the experimental dissociation of nitrogen (symbols) and the computed dissociation (solid lines).

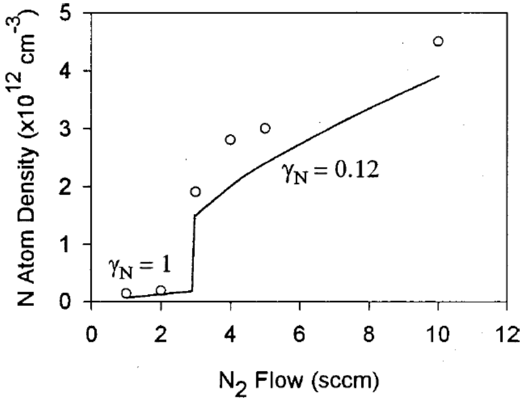

FIG. 4. The modeled atomic nitrogen density (solid line) is compared with experimental measurements (○) described in Ref. 11. The increase in [N] at 3 sccm is due to the experimentally observed transition from the metal target mode to the nitride target mode. The transition is modeled by decreasing the N wall loss parameter from $\gamma_N = 1$ to $\gamma_N = 0.12$. Plasma conditions were 15 mTorr total pressure, 1 kW plasma power, and 1 kW target power.

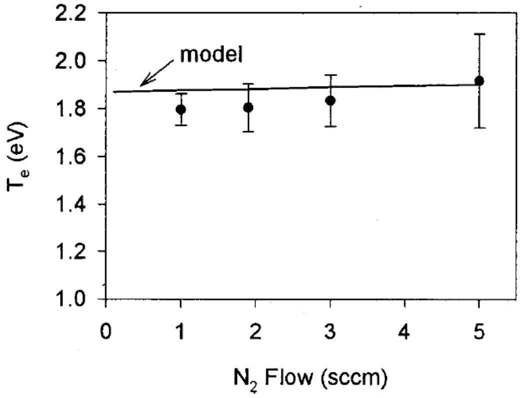

FIG. 5. Comparison of computed and measured electron temperature.

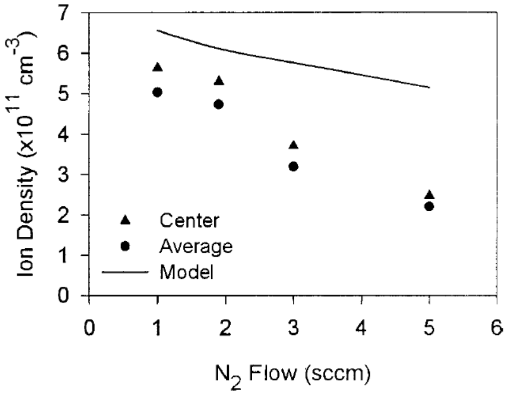

FIG. 6. Comparison of the computed global ion density with the ion density measured at the center of the discharge and the average ion density.

Tao, Mao, and Hopwood, J. Appl. Phys. 91, 4040 (2002)

Liang – 60 MHz N_2 Capacitively Coupled Plasma – Model

- Liang *et al.* developed a 2D fluid model of N_2 capacitively coupled plasma (CCP) operating at 60 MHz.
- The model was tested against experimentally measured N_2^+ ion density.
- Model was used to understand the effect of RF power and inter-electrode gap on plasma uniformity.

60 MHZ CCP

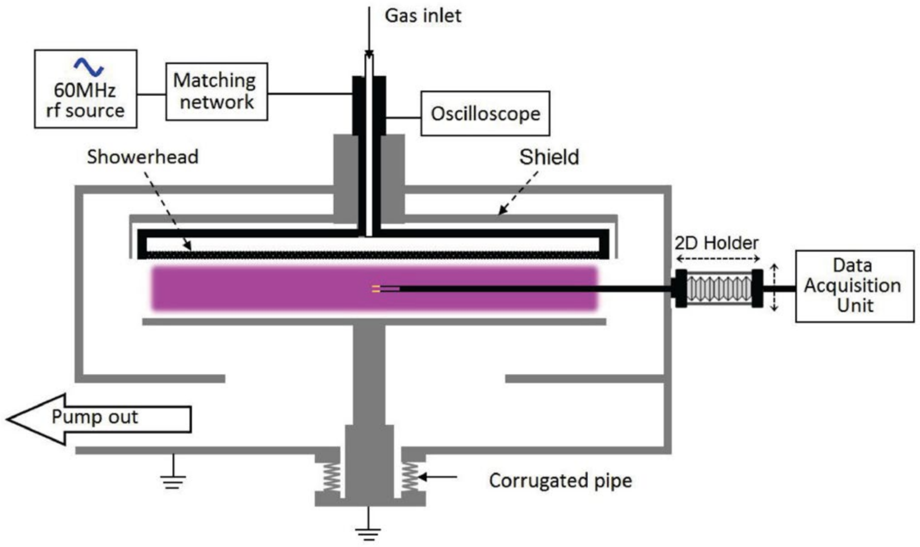

N_2 Plasma Chemistry

TABLE I. The reactions taken into account in the model.

No.	Reactions	Rate Coefficient[a]	ε[b]	Reference
R1	$N_2 + e \rightarrow N_2 + e$	$1.04 \times 10^{-7}(T_e)^{0.43} \exp(-0.206/T_e)$[c]		29
R2	$N + e \rightarrow N^+ + 2e$	$3.87 \times 10^{-9}(T_e)^{0.86} \exp(-14.62/T_e)$[c]	14.54	29
R3	$N_2 + e \rightarrow N_2^+ + 2e$	$7.76 \times 10^{-9}(T_e)^{0.79} \exp(-16.75/T_e)$[c]	15.60	29
R4	$N_2 + e \rightarrow N_2(A) + e$	$8.06 \times 10^{-10}(T_e)^{-0.306} \exp(-8.87/T_e)$[c]	6.17	29
R5	$N_2 + e \rightarrow N_2(B) + e$	$1.56 \times 10^{-8}(T_e)^{-0.52} \exp(-9.16/T_e)$[c]	7.35	29
R6	$N_2 + e \rightarrow N_2(a') + e$	$6.6 \times 10^{-9}(T_e)^{-0.66} \exp(-11.05/T_e)$[c]	8.40	29
R7	$N_2^+ + e \rightarrow N + N$	$1.8 \times 10^{-7}(T_e)^{-0.39}$[c]		15
R8	$N_2 + e \rightarrow N + N + e$	$2.15 \times 10^{-8} \exp(-14.39/T_e)$[c]	9.75	30
R9	$N_2(A) + N_2(a') \rightarrow N_2^+ + N_2 + e$	3.2×10^{-12}		31
R10	$N_2(a') + N_2(a') \rightarrow N_2^+ + N_2 + e$	5.0×10^{-11}		32
R11	$N_2^+ + N \rightarrow N^+ + N_2$	$7.21 \times 10^{-13} \exp(T_{gas}/300.0)$[d]		31
R12	$N_2(A) + N \rightarrow N_2 + N$	2.0×10^{-12}		31
R13	$N_2(A) + N_2 \rightarrow N_2 + N_2$	3.0×10^{-18}		33
R14	$N_2(A) + N_2(A) \rightarrow N_2(B) + N_2$	7.7×10^{-11}		16
R15	$N_2(B) + N_2 \rightarrow N_2(X_{v=0}) + N_2$	1.5×10^{-12}		34
R16	$N_2(B) + N_2 \rightarrow N_2(A) + N_2$	2.85×10^{-11}		34
R17	$N_2(a') + N_2 \rightarrow N_2(B) + N_2$	1.9×10^{-13}		16
R18	$N + N + N \rightarrow N_2(B) + N_2$	$8.27 \times 10^{-34} exp(500.0/T_{gas})$[d,e]		16
R19	$N + N + N_2 \rightarrow N_2 + N$	1.0×10^{-32}[e]		33
R20	$N_2(B) \rightarrow N_2(A) + h\nu$	2.0×10^{5}[f]		16

Liang *et al.*, J. Appl. Phys. 117, 083301 (2015)

Liang – 60 MHz N_2 Capacitively Coupled Plasma – Plasma Uniformity

- The model showed that plasma intensified closer to the electrode edge as power increased.
- Plasma uniformity worsening with power linked to P_r at electrode edge increasing more rapidly than P_z.
- Demonstrated using model that inter-electrode gap can be increased to improve plasma uniformity.

N_2^+ Density

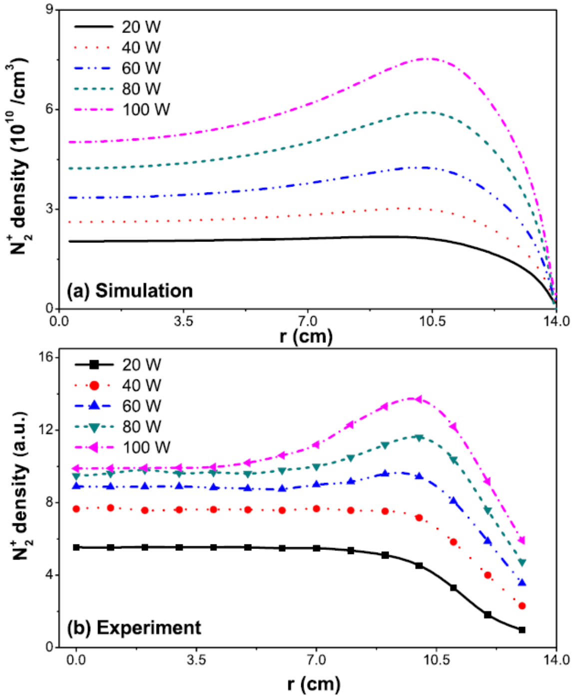

Power

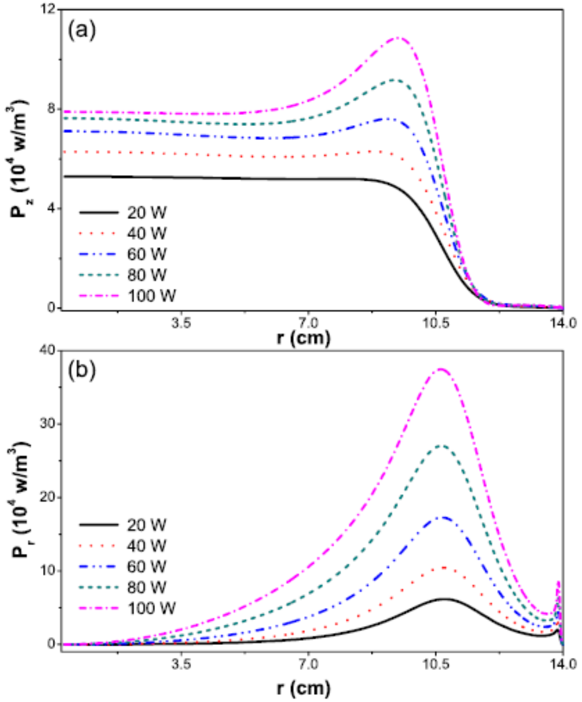

N_2^+ Density vs. Gap

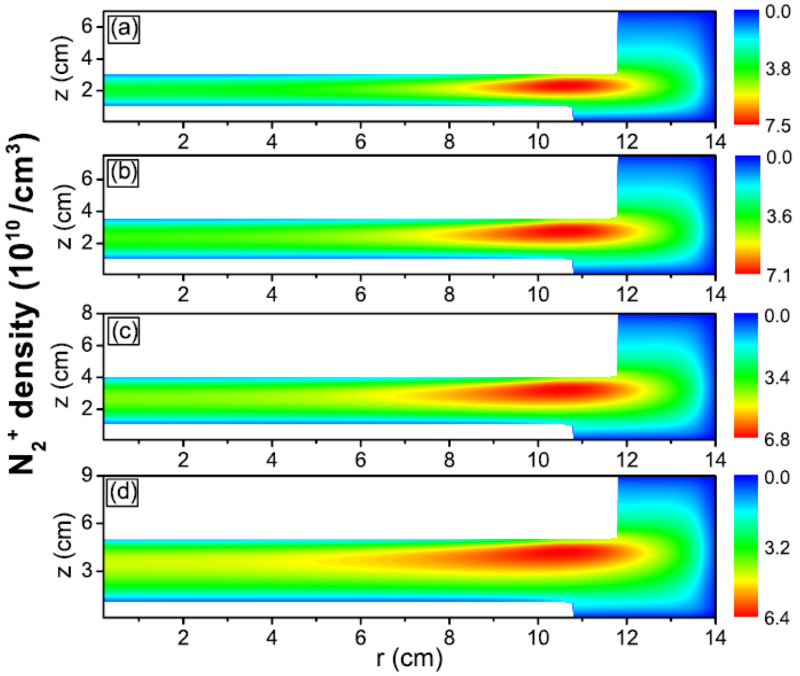

Liang *et al.*, J. Appl. Phys. 117, 083301 (2015)

APPLIED MATERIALS

Wang – Uniformity Control in Capacitive Discharge – Model

- Wang *et al.* used a 2D PIC/MCC model to simulate a cylindrical 13.56 MHz CCP.
- Examined the effect of introducing trenches in the top (grounded) and bottom (powered electrode).
- Simulations done for Ar plasma, 10 Pa, 1024 points in radial + axial directions, and > 7 million particles.

Chamber Geometry

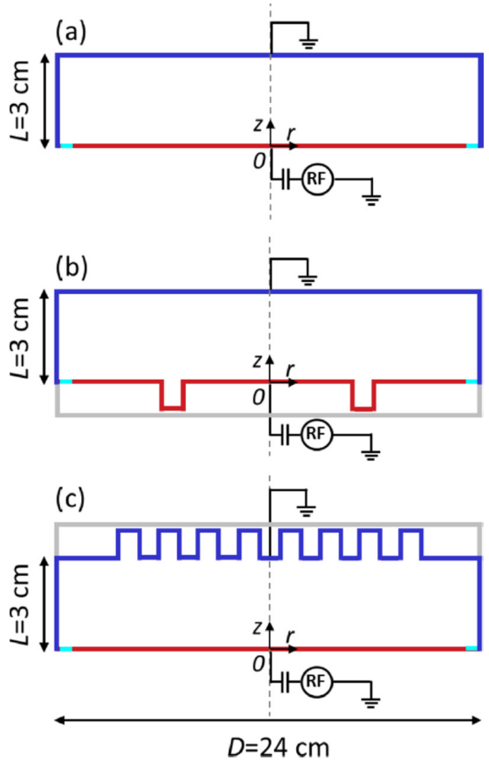

Electron Density

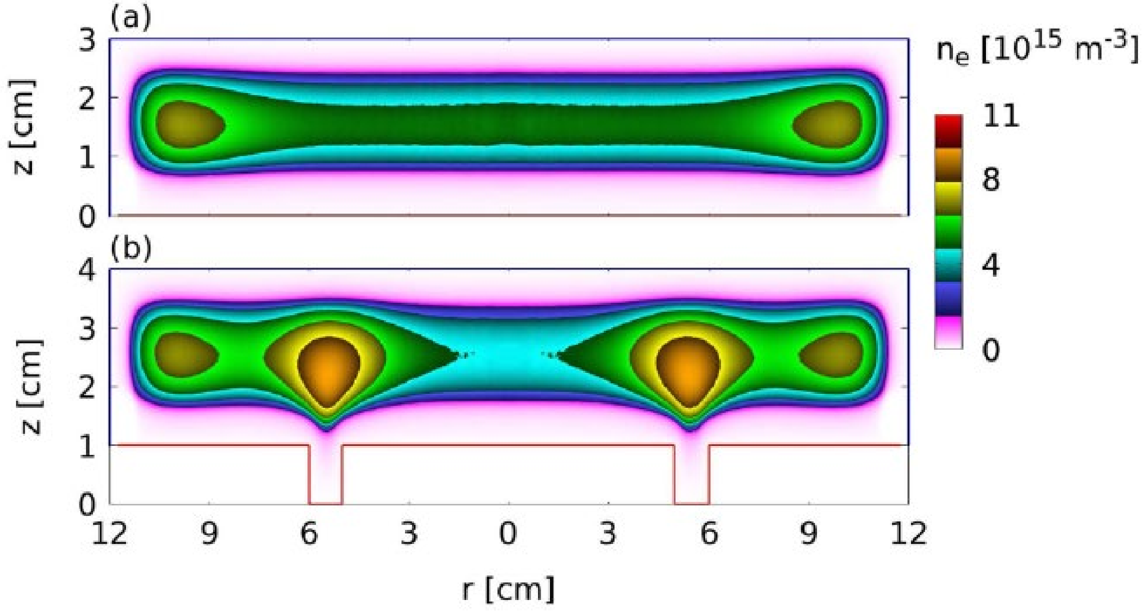

Wang *et al.*, J. Vac. Sci. Technol. A 39, 063004 (2021)

Wang – Uniformity Control in Capacitive Discharge – Testing New Concept

- The plasma density peaked at chamber edge due to strong electron heating at powered electrode edge.
- Found that electron heating enhances near trench corners, intensifying the plasma in the trench's vicinity.
- Demonstrated that multiple ring-shaped trenches can be used to improve the plasma uniformity.

Electron Density

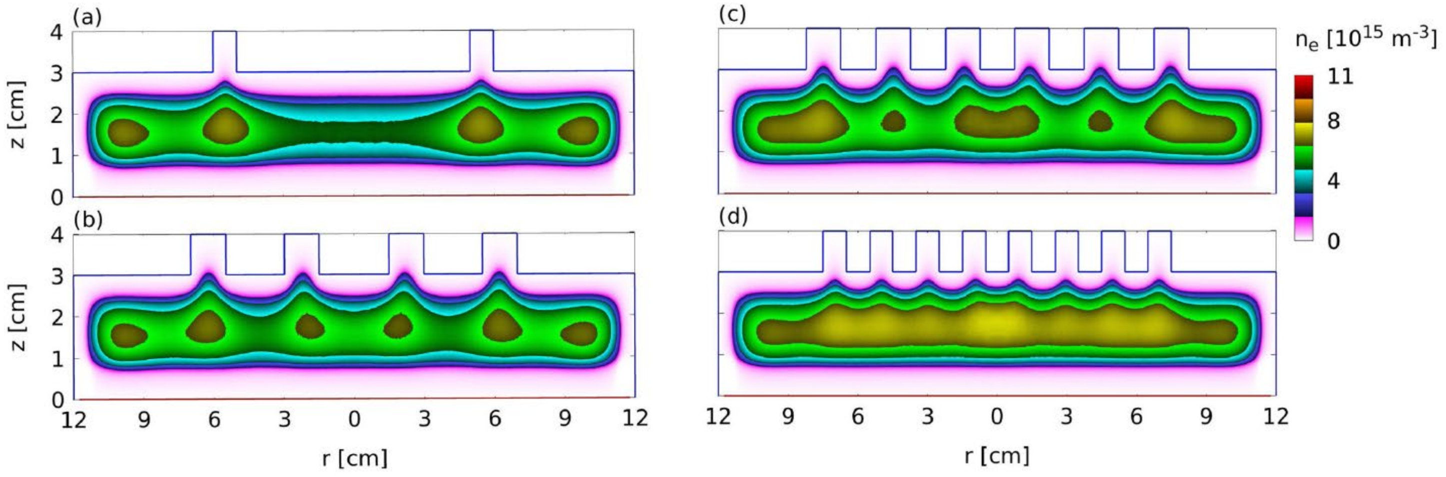

Electron Density vs. r

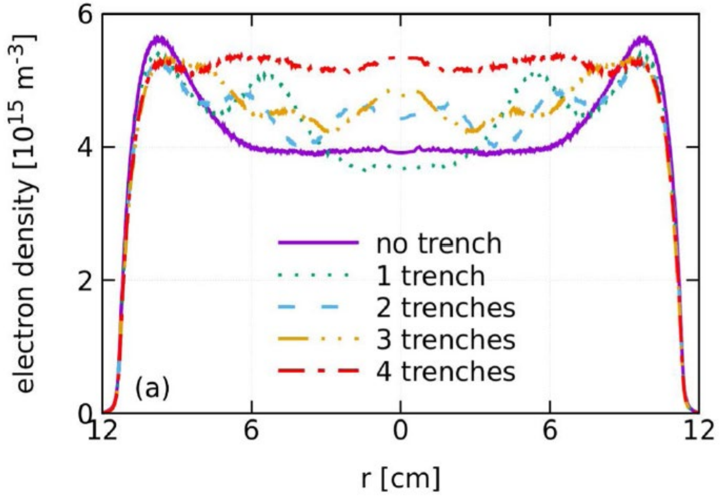

Wang *et al.*, J. Vac. Sci. Technol. A 39, 063004 (2021)

Babaeva – Plasma at Wafer Edge – Model

- Babaeva and Kushner examined the effect of the gap between wafer and focus ring.
- 2D simulations of the CCP discharge were done using nonPDPSIM, a fluid plasma model.
- Simulations were done for Ar/CF_4 plasma at 90 mTorr with 10 MHz power.

Dies on Wafer

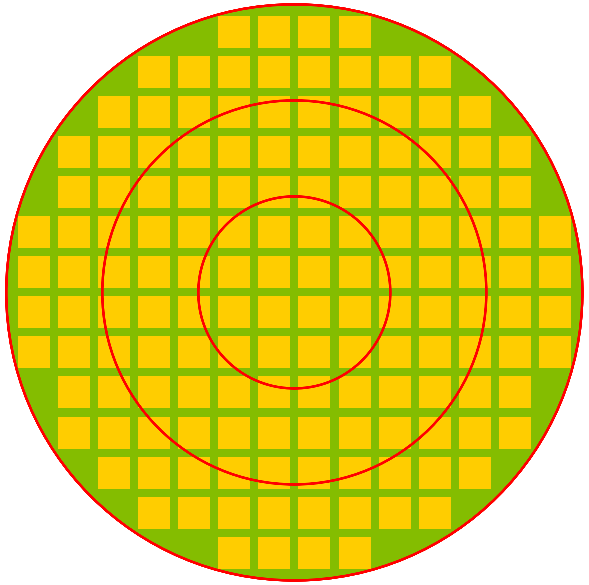

Chamber Geometry

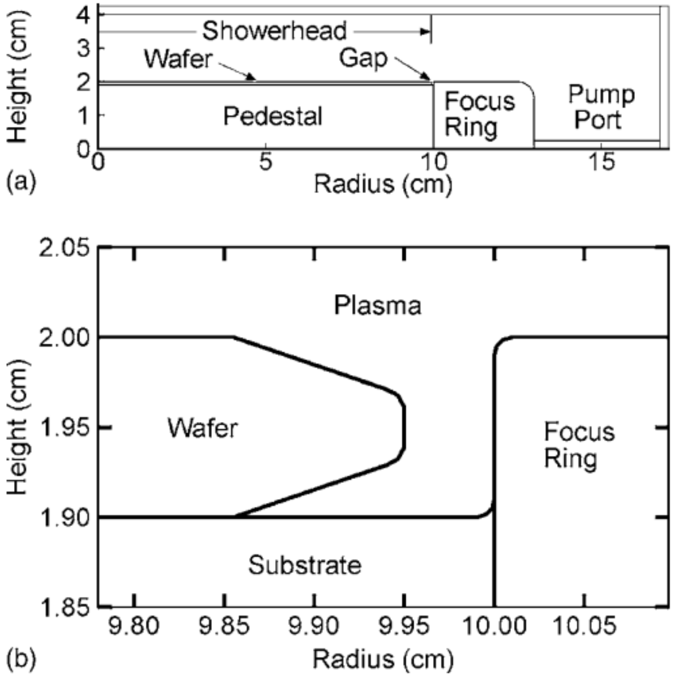

Ar/CF_4 Chemistry

TABLE I. Reduced reaction mechanism for Ar/CF_4 plasmas.

Species		
Ar	CF_4	CF_3^+
$Ar^*(4s)$	CF_3	CF_3^-
$Ar^{**}(4p)$	CF_2	F^-
Ar^+	CF	e
	F_2	
	F	

Reactions[a]	Rate coefficient[b]	Reference
Electron Impact:		
$e+Ar \rightarrow Ar^*+e$	c	10
$e+Ar \rightarrow Ar^{**}+e$	c	10
$e+Ar \rightarrow Ar^++e+e$	c	11
$e+Ar^* \rightarrow Ar^++e+e$	c	12
$e+Ar^* \rightarrow Ar+e$	c	10
$e+Ar^* \rightarrow Ar^{**}+e$	c	13
$e+Ar^{**} \rightarrow Ar+e$	c	10
$e+Ar^{**} \rightarrow Ar^++e$	c	14
$e+Ar^{**} \rightarrow Ar^*+e$	c	13
$e+CF_4 \rightarrow CF_3+F^-$	c	15
$e+CF_4 \rightarrow CF_3^-+F$	c	15
$e+CF_4 \rightarrow CF_3+F+e$	c	15
$e+CF_4 \rightarrow CF_3^++F+e+e$	c	15[d]
$e+CF_4 \rightarrow CF_2+F+F+e$	c	15
$e+CF_4 \rightarrow CF_3^++F^-+e$	c	15
$e+CF_4 \rightarrow CF+F+F_2+e$	c	15
$e+CF_3 \rightarrow CF_2+F+e$	c	15[f]
$e+CF_3 \rightarrow CF_3^++e+e$	c	16
$e+CF_3 \rightarrow CF_2+F^-$	c	15[f]
$e+CF_2 \rightarrow CF+F^-$	c	15[f]
$e+CF_2 \rightarrow CF+F+e$	c	15[f]
$e+F_2 \rightarrow F^-+F$	c	17
Neutral heavy particle reactions:		
$Ar^*+Ar^* \rightarrow Ar^++Ar+e$	1.0×10^{-9}	18
$Ar^{**}+Ar^{**} \rightarrow Ar^++Ar+e$	1.0×10^{-9}	18
$Ar^{**}+Ar^* \rightarrow Ar^++Ar+e$	1.0×10^{-9}	18
$Ar^{**} \rightarrow Ar^*$	$2\times10^{6}\ s^{-1}$	e
$F+CF_3 \rightarrow CF_4$	2.0×10^{-11}	19
$F+CF_2 \rightarrow CF_3$	1.8×10^{-11}	20
$F+CF \rightarrow CF_2$	9.96×10^{-11}	21
$F_2+CF_2 \rightarrow CF_3+F$	8.3×10^{-14}	22
$F_2+CF_3 \rightarrow CF_4+F$	1.88×10^{-14}	21
$Ar^*+CF_4 \rightarrow CF_2+F_2+Ar$	4.0×10^{-11}	23
$Ar^*+CF_3 \rightarrow CF_2+F+Ar$	4.0×10^{-11}	23[f]
$Ar^*+CF_2 \rightarrow CF+F+Ar$	4.0×10^{-11}	23[f]
Ion-neutral particle reactions:		
$Ar^++Ar \rightarrow Ar+Ar^+$	4.6×10^{-10}	24
$CF_3^++CF_3 \rightarrow CF_3+CF_3^+$	1.0×10^{-9}	25
$CF_3^-+F \rightarrow CF_3+F^-$	5.0×10^{-8}	26
$F^-+CF_3 \rightarrow CF_4+e$	4.0×10^{-10}	27
$F^-+CF_2 \rightarrow CF_3+e$	3.0×10^{-10}	27
$F^-+CF \rightarrow CF_2+e$	2.0×10^{-10}	27
$F^-+F \rightarrow F_2+e$	1.0×10^{-10}	27
$Ar^++CF_4 \rightarrow CF_3^++Ar+F$	4.8×10^{-10}	28
$Ar^++CF_3 \rightarrow CF_3^++Ar$	7.0×10^{-10}	28[f]
Electron-ion and ion-ion reactions:		
$e+Ar^+ \rightarrow Ar^{**}$	$4.0\times10^{-13}T_e^{-0.5}$	29
$e+CF_3^+ \rightarrow CF_2+F$	$3.0\times10^{-8}T_e^{-0.5}$	g
$CF_3^-+CF_3^+ \rightarrow CF_3+CF_3$	3.0×10^{-7}	30
$F^-+CF_3^+ \rightarrow CF_2+F_2$	8.7×10^{-8}	25
$F^-+CF_3^+ \rightarrow CF_2+F+F$	$3.0\times10^{-7}(T/300)^{-0.5}$	27
$F^-+CF_3^+ \rightarrow F+CF_3$	3.0×10^{-7}	25
$CF_3^-+Ar^+ \rightarrow CF_3+Ar$	3.0×10^{-7}	30

Babaeva and Kushner, J. Appl. Phys. 101, 113307 (2007)

Babaeva – Plasma at Wafer Edge – Results

- As wafer edge – focus ring gap increased from 0.25 → 1 mm, the plasma reached below the wafer edge.
- Demonstrated that height of focus ring can be used to control plasma penetration under the wafer edge.

Potential vs. Time

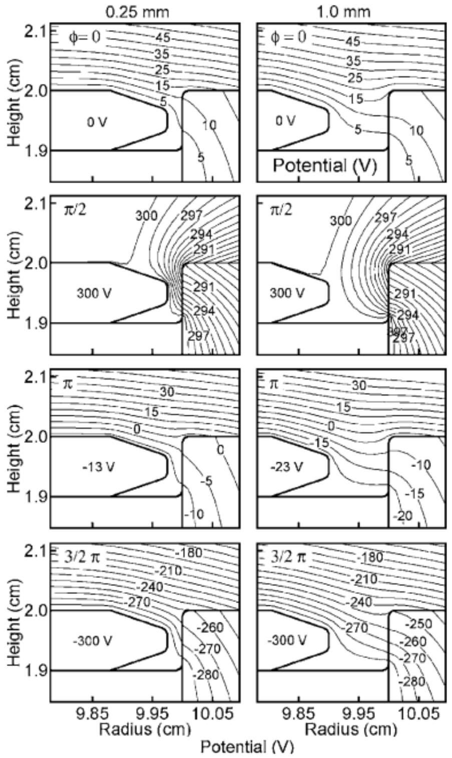

Effect of Gap

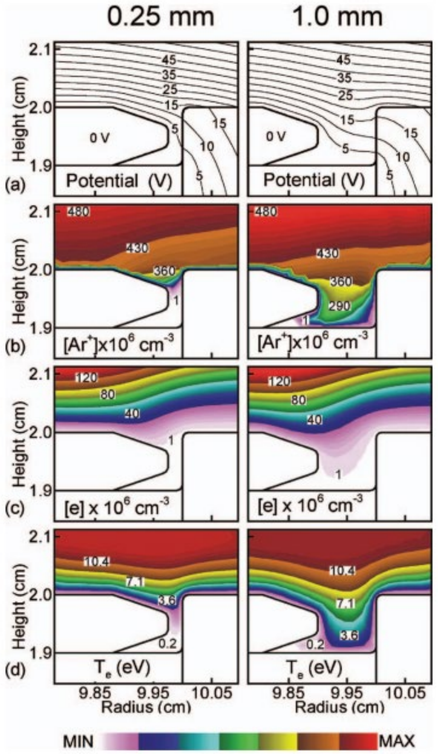

Effect of Ring Height

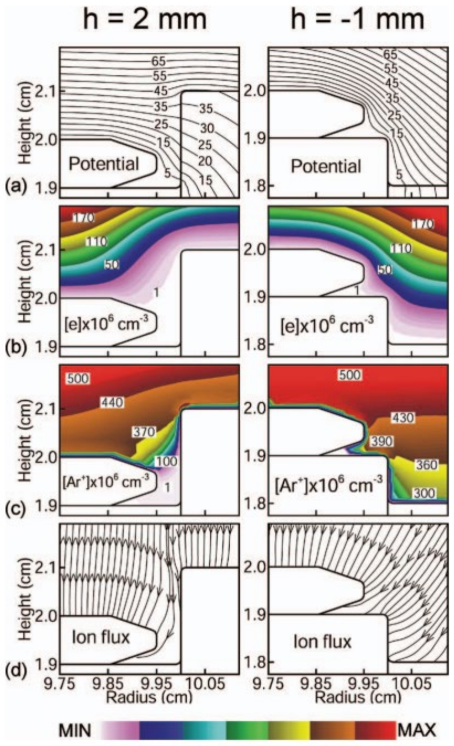

Babaeva and Kushner, J. Appl. Phys. 101, 113307 (2007)

APPLIED MATERIALS

Son – Plasma Breakdown in Narrow Gap – Model

- Reliability is key for industrial products. Helping fix issues in an important part of engineers' job.
- This includes unintended gas breakdown in regions that should be plasma-free.
- Son *et al.* studied gas breakdown in narrow gaps which are exposed to the main plasma volume.
- EDIPIC was used to do 2D PIC/MCC simulations in Ar at 5 Torr. Δx = 5 μm, Δt = 4 ps.

Geometry

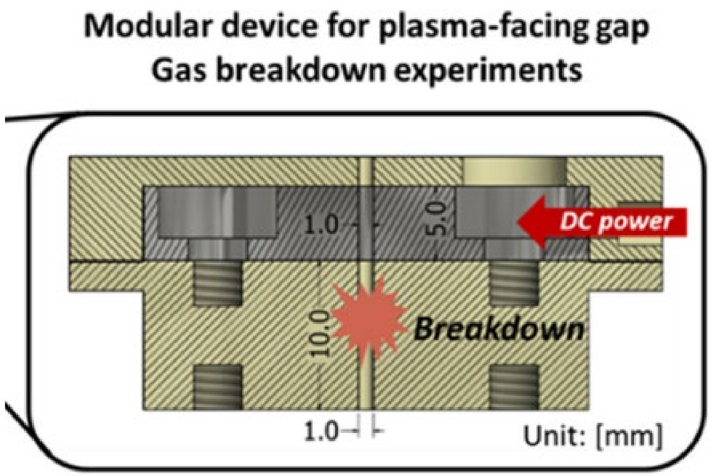

Breakdown Voltage vs. Pressure

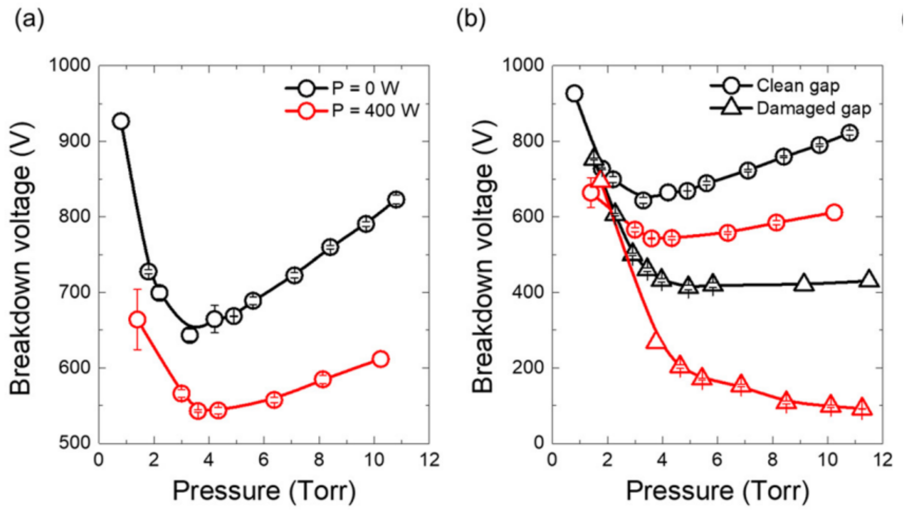

Damaged Material

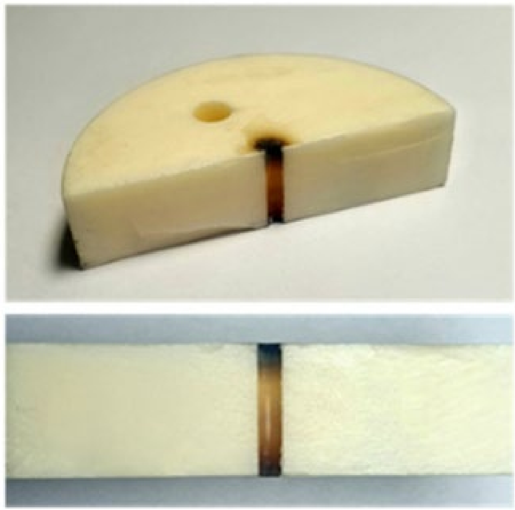

Son *et al.*, Appl. Phys. Lett. 123, 232108 (2023)

Son – Plasma Breakdown in Narrow Gap – Results

- They demonstrated that presence of low-density electrons in the gap significantly lowers the breakdown voltage.

Plasma Ignition

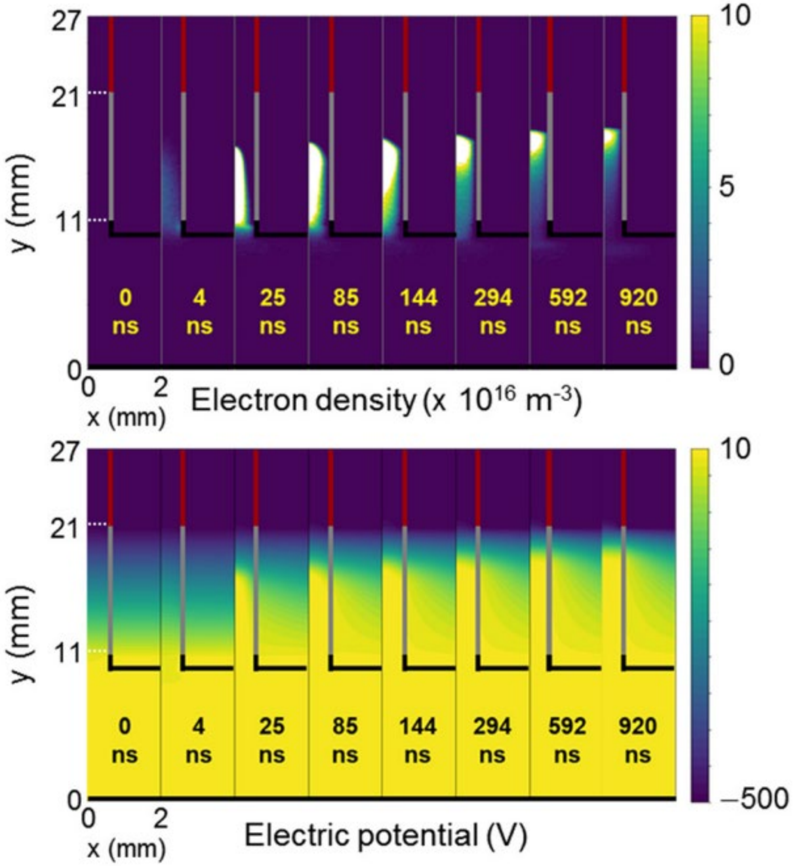

Breakdown Voltage

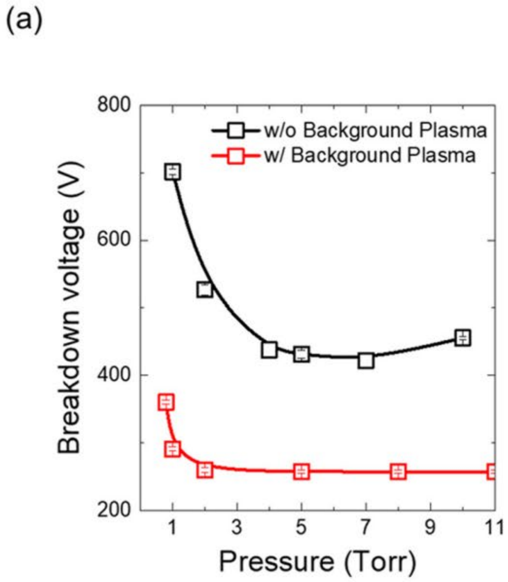

Density vs. Time

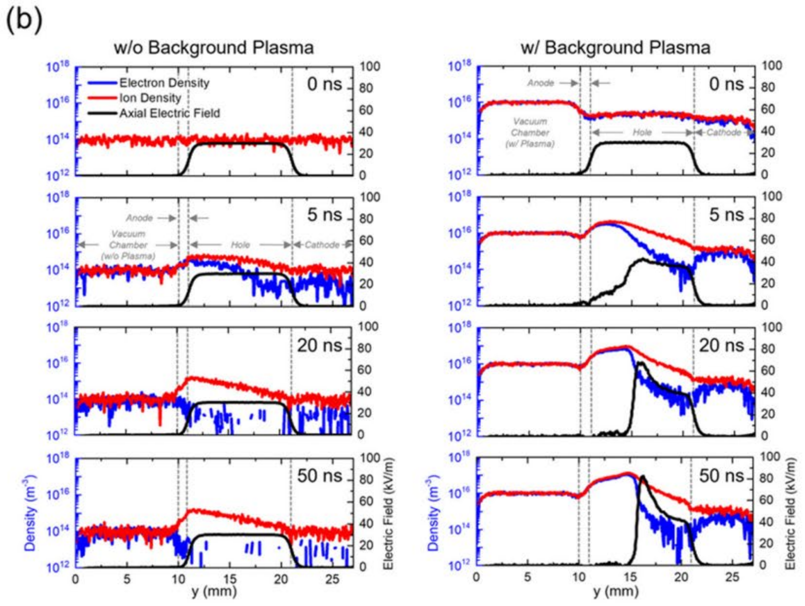

Son *et al.*, Appl. Phys. Lett. 123, 232108 (2023)

Huang – HAR Dielectric Etch – Model

- Huang *et al.* used a coupled plasma + feature scale model to examine high aspect ratio (HAR) dielectric etch.
- Plasma model: HPEM, feature scale model: MCFPM (University of Michigan).
- The model included detailed chemistry for $Ar/C_4F_8/O_2$ and a detailed mechanism for SiO_2 etch.

Plasma Properties

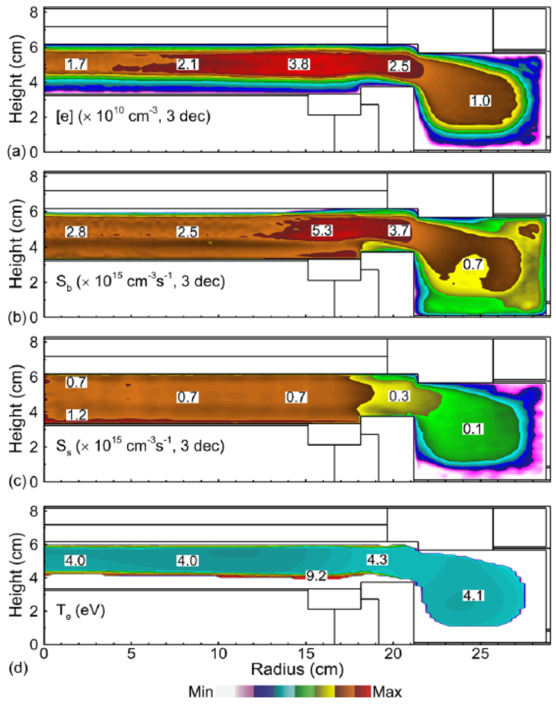

SiO_2 Etch Mechanism

TABLE I. Surface reaction mechanism for plasma etching of SiO_2 in $Ar/C_4F_8/O_2$ mixtures.

Gas phase species		Notes
Ions, hot neutrals, and neutral partners	Ar^+, Ar(h), Ar	a
	F^+, F(h), F	
	F_2^+, F_2(h), F_2	
	O^+, O(h), O	
	O_2^+, O_2(h), O_2	
	$C_mF_n^+$, C_mF_n(h), C_mF_n	
Etch products	CO, CO_2, COF, COH	
	SiF_x, SiF_4	b
Sputtered materials	R, SiO_2, Si	c

Surface sites		Notes
Photoresist	R(s)	
Silicon oxide	SiO_2(s)	
Passivated oxide surface (complex)	$SiO_2C_mF_n$(s)	d
	$SiOCF_3$(s)	
Silicon	Si(s)	
Fluorinated silicon surface	SiF_x(s)	e
Polymer	P(s)	
Activated surface sites	SiO_2^*(s)	f
	$SiO_2C_mF_n^*$(s)	
	$SiOCF_3^*$(s)	
	P^*(s)	

Reactions[g]	p_0[h]	E_{th} (eV)[h]	E_r (eV)[h]	Notes
Activation of SiO_2				
$SiO_2(s) + I^+ \rightarrow SiO_2^*(s) + I(h)$	0.9			i
Sputtering of SiO_2				
$SiO_2(s) + I^+ \rightarrow SiO_2 + I(h)$	0.9	70	140	i,j
$SiO_2^*(s) + I^+ \rightarrow SiO_2 + I(h)$	0.9	70	140	i,j
Passivation of SiO_2				
$SiO_2(s) + CF \rightarrow SiO_2CF(s)$	0.4			Ref. 39
$SiO_2(s) + CF_2 \rightarrow SiO_2CF_2(s)$	0.3			Ref. 39
$SiO_2(s) + CF_3 \rightarrow SiO_2CF_3(s)$	0.2			Ref. 39
$SiO_2(s) + C_2F_3 \rightarrow SiO_2C_2F_3(s)$	0.2			Ref. 39,k
$SiO_2^*(s) + CF_x \rightarrow SiO_2CF_x(s)$	0.9			k,l
$SiO_2^*(s) + C_2F_3 \rightarrow SiO_2C_2F_3(s)$	0.9			k
Further passivation of complex				
$SiO_2CF(s) + CF_2 \rightarrow SiO_2C_2F_3(s)$	10^{-4}			
$SiO_2CF_2(s) + CF \rightarrow SiO_2C_2F_3(s)$	10^{-4}			
$SiO_2CF_2(s) + CF_2 \rightarrow SiO_2C_2F_4(s)$	10^{-4}			
$SiO_2CF_2(s) + C_2F_3 \rightarrow SiO_2C_3F_5(s)$	10^{-4}			
$SiO_2CF_3(s) + CF \rightarrow SiO_2C_2F_4(s)$	10^{-4}			
$SiO_2CF_3(s) + C_2F_3 \rightarrow SiO_2C_3F_6(s)$	10^{-4}			
$SiO_2C_2F_3(s) + CF_2 \rightarrow SiO_2C_3F_5(s)$	10^{-4}			
$SiO_2C_2F_4(s) + CF \rightarrow SiO_2C_3F_5(s)$	10^{-4}			
$SiO_2C_2F_4(s) + CF_2 \rightarrow SiO_2C_3F_6(s)$	10^{-4}			
Fluorination of passivated surface				
$SiO_2CF(s) + F \rightarrow SiO_2CF_2(s)$	0.1			
$SiO_2CF_2(s) + F \rightarrow SiO_2CF_3(s)$	0.1			
$SiO_2C_2F_3(s) + F \rightarrow SiO_2C_2F_4(s)$	0.1			
$SiO_2C_3F_5(s) + F \rightarrow SiO_2C_3F_6(s)$	0.1			
Etching of passivated surface complex				
$SiO_2CF(s) + I^+ \rightarrow SiF + CO_2 + I(h)$	0.75	35	140	i,m
$SiO_2CF_2(s) + I^+ \rightarrow SiF_2 + CO_2 + I(h)$	0.75	35	140	i,m
$SiO_2CF_3(s) + I^+ \rightarrow SiF_3 + CO_2 + I(h)$	0.75	35	140	i,m
$SiO_2C_2F_3(s) + I^+ \rightarrow SiOCF_3(s) + CO + I(h)$	0.75	35	140	i,m
$SiO_2C_2F_4(s) + I^+ \rightarrow SiOCF_3(s) + COF + I(h)$	0.75	35	140	i,m
$SiO_2C_3F_5(s) + I^+ \rightarrow SiO_2CF(s) + C_2F_4 + I(h)$	0.75	35	140	i,m

TABLE I. Continued

Reactions[g]	p_0[h]	E_{th} (eV)[h]	E_r (eV)[h]	Notes
$SiO_2C_3F_6(s) + I^+ \rightarrow SiO_2CF_3(s) + C_2F_3 + I(h)$	0.75	35	140	i,m
$SiOCF_3(s) + I^+ \rightarrow SiF_3 + CO + I(h)$	0.75	35	140	i,m
$SiO_2CF^*(s) + I^+ \rightarrow SiF + CO_2 + I(h)$	0.75	35	140	i,m
$SiO_2CF_2^*(s) + I^+ \rightarrow SiF_2 + CO_2 + I(h)$	0.75	35	140	i,m
$SiO_2CF_3^*(s) + I^+ \rightarrow SiF_3 + CO_2 + I(h)$	0.75	35	140	i,m
$SiO_2C_2F_3^*(s) + I^+ \rightarrow SiOCF_3(s) + CO + I(h)$	0.75	35	140	i,m
$SiO_2C_2F_4^*(s) + I^+ \rightarrow SiOCF_3(s) + COF + I(h)$	0.75	35	140	i,m
$SiO_2C_3F_5^*(s) + I^+ \rightarrow SiO_2CF(s) + C_2F_4 + I(h)$	0.75	35	140	i,m
$SiO_2C_3F_6^*(s) + I^+ \rightarrow SiO_2CF_3(s) + C_2F_3 + I(h)$	0.75	35	140	i,m
$SiOCF_3^*(s) + I^+ \rightarrow SiF_3 + CO + I(h)$	0.75	35	140	i,m
Polymer deposition on activated complex				
$SiO_2C_mF_n^*(s) + CF \rightarrow SiO_2C_mF_n^*(s) + P(s)$	0.002			
$SiO_2C_mF_n^*(s) + CF_2 \rightarrow SiO_2C_mF_n^*(s) + P(s)$	0.0015			
$SiO_2C_mF_n^*(s) + CF_3 \rightarrow SiO_2C_mF_n^*(s) + P(s)$	0.001			
$SiO_2C_mF_n^*(s) + C_xF_y \rightarrow SiO_2C_mF_n^*(s) + P(s)$	0.001			k
$SiOCF_3^*(s) + CF \rightarrow SiOCF_3^*(s) + P(s)$	0.002			
$SiOCF_3^*(s) + CF_2 \rightarrow SiOCF_3^*(s) + P(s)$	0.0015			
$SiOCF_3^*(s) + CF_3 \rightarrow iOCF_3^*(s) + P(s)$	0.001			
$SiOCF_3^*(s) + C_xF_y \rightarrow SiOCF_3^*(s) + P(s)$	0.001			k
Polymer deposition on polymer				
$P(s) + CF \rightarrow P(s) + P(s)$	0.002			
$P(s) + CF_2 \rightarrow P(s) + P(s)$	0.0015			
$P(s) + CF_3 \rightarrow (s) + P(s)$	0.001			
$P(s) + C_xF_y \rightarrow P(s) + P(s)$	0.001			k
$P^*(s) + CF \rightarrow P^*(s) + P(s)$	0.02			
$P^*(s) + CF_2 \rightarrow P^*(s) + P(s)$	0.015			
$P^*(s) + CF_3 \rightarrow P^*(s) + P(s)$	0.01			
$P^*(s) + C_xF_y \rightarrow P^*(s) + P(s)$	0.01			k
Polymer chemical sputtering				
$P(s) + I^+ \rightarrow I(h) + CF_2$	0.3	30	140	j,n
$P^*(s) + I^+ \rightarrow I(h) + CF_2$	0.3	30	140	j,n
$P(s) + O^+ \rightarrow COF$	0.2	20	100	m
$P(s) + O_2^+ \rightarrow O(h) + COF$	0.2	20	100	m
$P^*(s) + O^+ \rightarrow COF$	0.2	20	100	m
$P^*(s) + O_2^+ \rightarrow O(h) + COF$	0.2	20	100	m
Polymer chemical erosion				
$P(s) + F \rightarrow CF_2$	0.001			
$P^*(s) + F \rightarrow CF_2$	0.03			
$P(s) + O \rightarrow COF$	0.5			
$P^*(s) + O \rightarrow COF$	0.9			
Fluorination and etching of Si				
$Si(s) + F \rightarrow SiF(s)$	0.01			
$SiF(s) + F \rightarrow SiF_2(s)$	0.02			
$SiF_2(s) + F \rightarrow SiF_3(s)$	0.03			
$SiF_3(s) + F \rightarrow SiF_4$	0.05			
Chemical, physical sputtering Si(s), SiF_x(s)				
$Si(s) + I^+ \rightarrow Si + I(h)$	0.1	37.5	100	Ref. 40,i,j
$SiF(s) + I^+ \rightarrow SiF + I(h)$	0.3	10	100	i,m
$SiF_2(s) + I^+ \rightarrow SiF_2 + I(h)$	0.4	10	100	i,m
$SiF_3(s) + I^+ \rightarrow SiF_3 + I(h)$	0.5	10	100	i,m
Polymer deposition on Si(s) and SiF_x(s)				
$Si(s) + CF \rightarrow Si(s) + P(s)$	0.5			
$Si(s) + CF_2 \rightarrow Si(s) + P(s)$	0.375			
$Si(s) + CF_3 \rightarrow Si(s) + P(s)$	0.25			
$Si(s) + C_xF_y \rightarrow Si(s) + P(s)$	0.25			k
$SiF_x(s) + CF \rightarrow SiF_x(s) + P(s)$	0.002			
$SiF_x(s) + CF_2 \rightarrow SiF_x(s) + P(s)$	0.0015			
$SiF_x(s) + CF_3 \rightarrow SiF_x(s) + P(s)$	0.001			
$SiF_x(s) + C_xF_y \rightarrow SiF_x(s) + P(s)$	0.001			k

TABLE I. Continued

Reactions[g]	p_0[h]	E_{th} (eV)[h]	E_r (eV)[h]	Notes
Redeposition of SiF_x				
$P(s) + SiF_x \rightarrow P(s) + SiF_x(s)$	0.001			
Erosion of photoresist				
$R(s) + I^+ \rightarrow R + I(h)$	0.01	20	100	i,j
$R(s) + O \rightarrow COH$	10^{-5}			
Redeposition of gas phase photoresist				
$W(s) + R \rightarrow W(s) + R(s)$	0.01			o
Polymer deposition on photoresist				
$R(s) + CF \rightarrow R(s) + P(s)$	0.02			
$R(s) + CF_2 \rightarrow R(s) + P(s)$	0.015			
$R(s) + CF_3 \rightarrow R(s) + P(s)$	0.01			
$R(s) + C_xF_y \rightarrow R(s) + P(s)$	0.01			k
	p_0[p]	E_{th} (eV)[p]	E_m (eV)[p]	Notes
Activation by low energy ions				
$SiO_2C_mF_n(s) + I^+ \rightarrow SiO_2C_mF_n^*(s) + I(h)$	0.1	5	70	i,j
$SiOCF_3(s) + I^+ \rightarrow SiOCF_3^*(s) + I(h)$	0.1	5	70	i,j
$P(s) + M^+ \rightarrow P^*(s) + M(h)$	0.3	5	30	i,j,q
Polymer deposition by low energy ions				
$SiO_2C_mF_n(s) + CF_x^+ \rightarrow SiO_2C_mF_n(s) + P(s)$	0.1	5	70	j,k
$SiO_2C_mF_n(s) + C_xF_y^+ \rightarrow SiO_2C_mF_n(s) + P(s)$	0.1	5	70	j,k
$SiOCF_3(s) + CF_x^+ \rightarrow SiOCF_3(s) + P(s)$	0.1	5	70	j,k
$SiOCF_3(s) + C_xF_y^+ \rightarrow SiOCF_3(s) + P(s)$	0.1	5	70	j,k

Huang *et al.*, J. Vac. Sci. Technol. A 37, 031304 (2019)

Huang – HAR Dielectric Etch – Feature Scale Results

- Simulations were used to understand how the etch process evolves with increasing aspect ratio (AR).
- Ions converted to "hot neutrals" when they impacted the sidewalls inside trenches.
- Power delivered to the feature bottom decreased with AR due to increased energy loss on sidewall impact.
- They demonstrated how the profile can be controlled by changing the ratio of C_xF_y neutrals to ions.

HAR Etch vs. Time

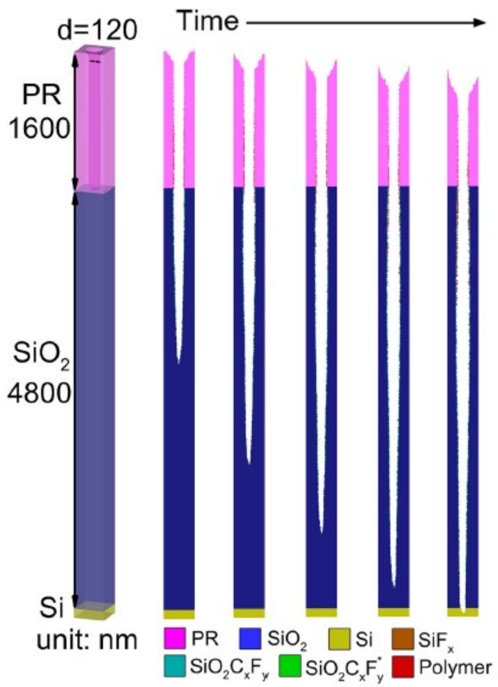

Ions and Hot Neutrals

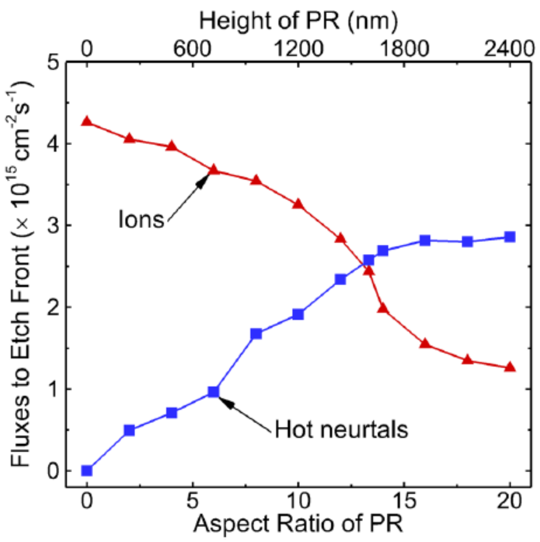

Power vs. Aspect Ratio

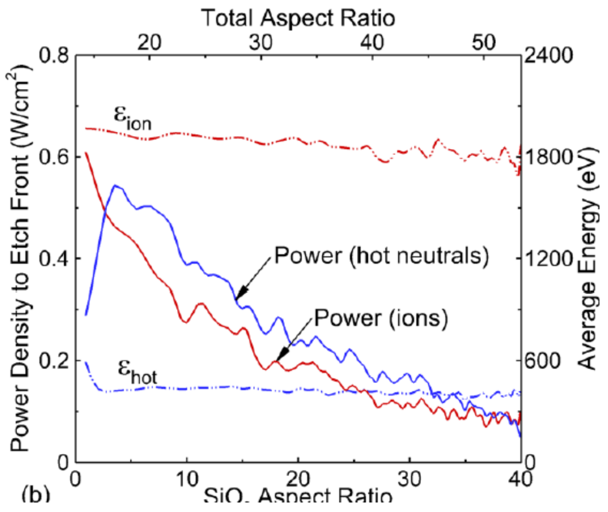

Huang *et al.*, J. Vac. Sci. Technol. A 37, 031304 (2019)

Huard – Si Atomic Layer Etch (ALE) – Feature Scale Results

- Huard *et al.* used the same codes (HPEM+MCFPM) to investigate Si ALE under non-ideal conditions.
- The found that high neutral / ion flux ratio is needed to get smooth surface during ALE.
- ALE during over-etching helps get clean fin profiles in less time with reduced damage.

Surface Roughness vs. Γ_i/Γ_n

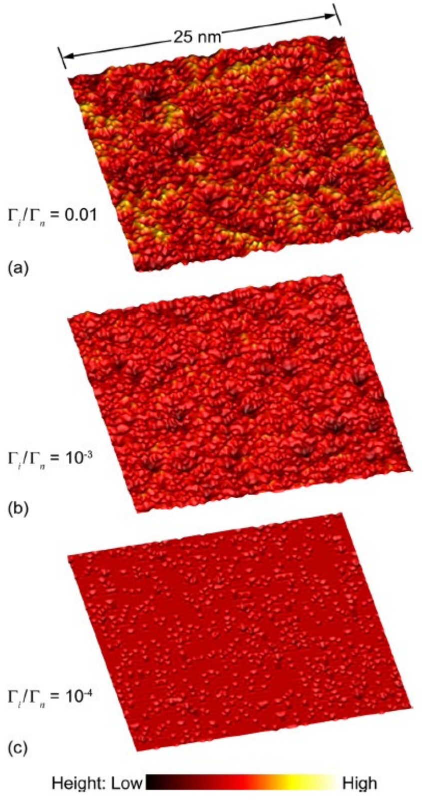

Profile During Etch

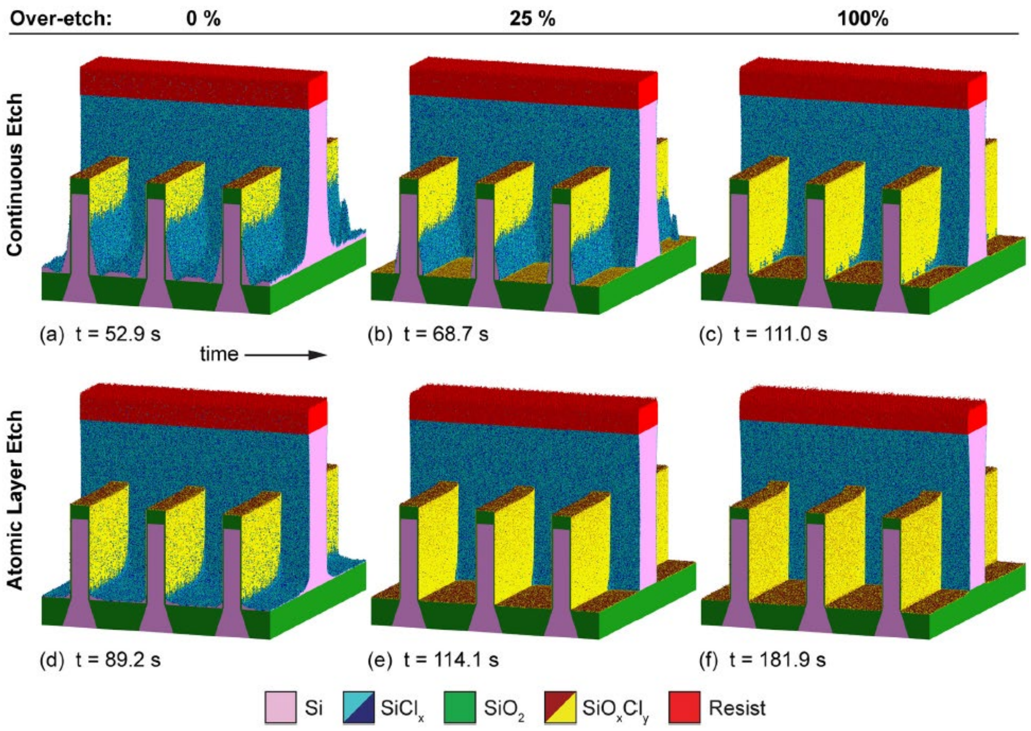

Huard *et al.*, J. Vac. Sci. Technol. A 35, 031306 (2017).

Kuboi – PECVD Feature Scale Model

- Kuboi *et al.* studied plasma enhanced CVD deposition of Si_3N_4 in $SiH_4/NH_3/N_2$ and SiH_4/N_2O.
- Experiments showed that, when deposited at 120° C, the film is columnar at low flow rate.
- Modeling was done using a Monte Carlo feature scale model that included surface migration.

Si_3N_4 PECVD at 120° C

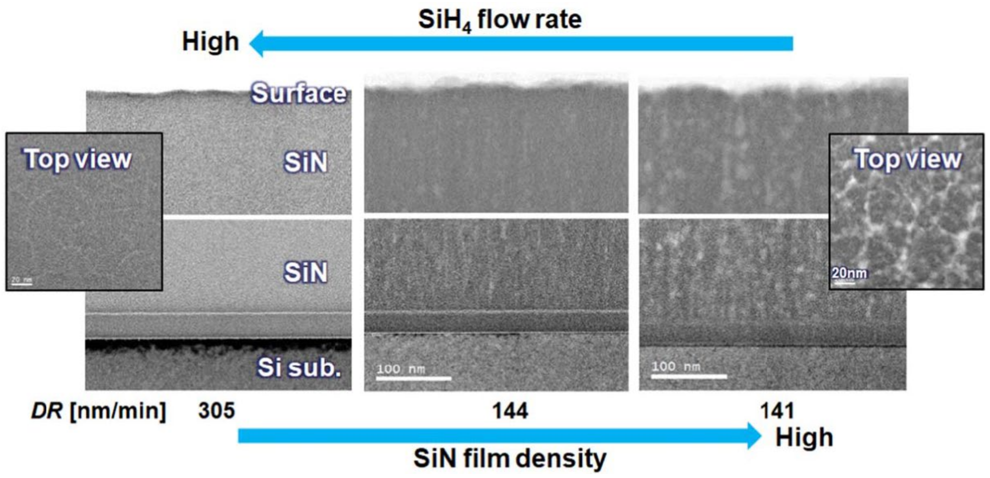

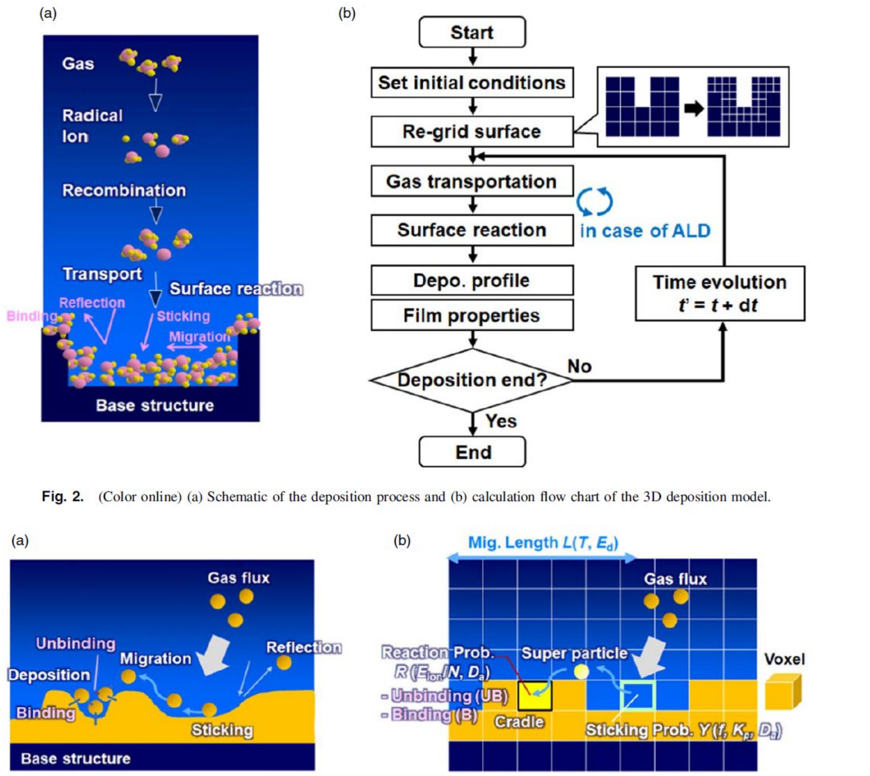

Fig. 2. (Color online) (a) Schematic of the deposition process and (b) calculation flow chart of the 3D deposition model.

Fig. 3. (Color online) Schematic pictures of (a) actual phenomena on the deposited surface over the base structure: irradiation of gas, sticking, reflection, migration, and binding and (b) corresponding deposition model using a statistical ensemble method in the voxel space.

Kuboi *et al.*, Jpn. J. App. Phys. 62, S11006 (2023)

Kuboi – PECVD Feature Scale Model

- The structure of the film vs. SiH_4 flow was attributed to recombination in gas phase.
- Longer residence time at lower SiH_4 flow led to formation of larger clusters in the gas, producing columnar film growth.

Evolution of Deposited Film

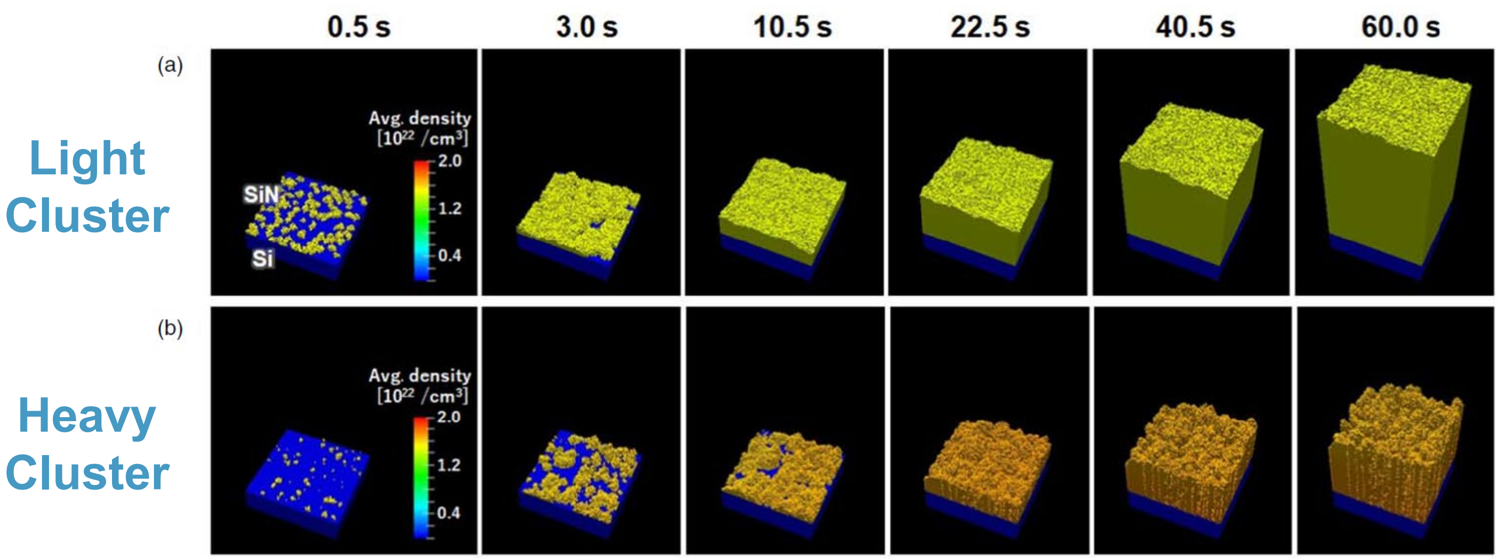

Film in Feature

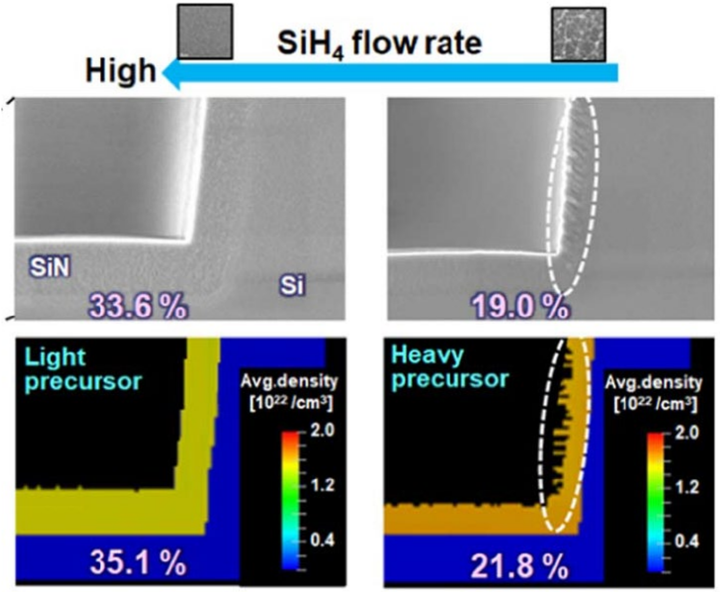

Kuboi *et al.*, Jpn. J. App. Phys. 62, S11006 (2023)

Vella – Si Atomic Layer Etch (ALE) – Molecular Dynamics (MD) Model

- Vella and Graves used a MD model to examine Si ALE in Cl_2 + Ar plasma.
- They used the REBO potential developed earlier in their group to model the Si-Cl system.
- Etch is self-limiting and close to ideal ALE at 25 eV. The etch rate is low.
- With increasing ion energy, etching does not stop during the etch step.

Ideal Si-Cl_2-Ar Atomic Layer Etch Process

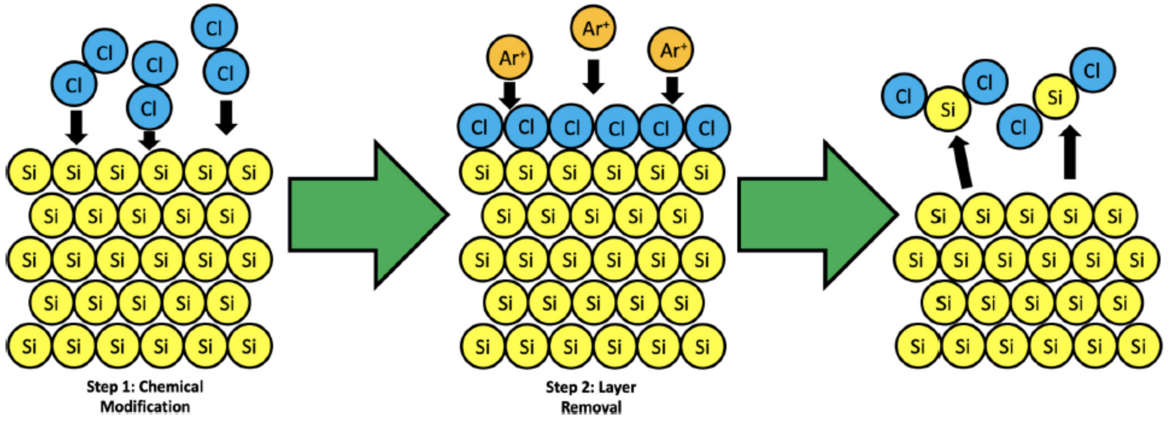

Si Etched vs. Time

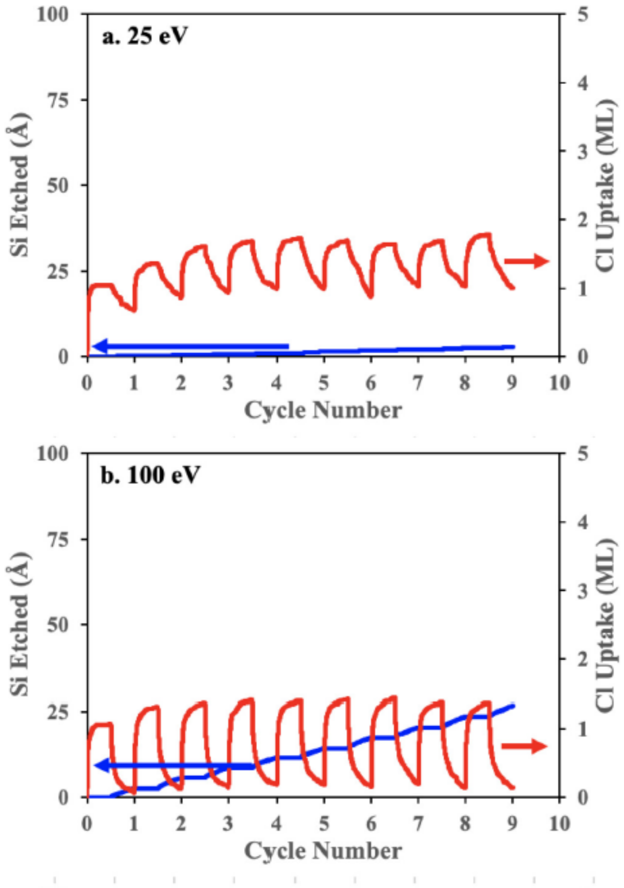

Vella and Graves, J. Vac. Sci. Technol. A 41, 042601 (2023)

Vella – Si ALE – MD Results

- It was shown that if multiple ions are used during the ion bombardment step, the structure seen by the ion changes with time. The last ions experience a more physical sputtering like condition.
- Ions create a mixed layer near the surface with some residual Cl.

Si Structure After Ar^+ Bombardment

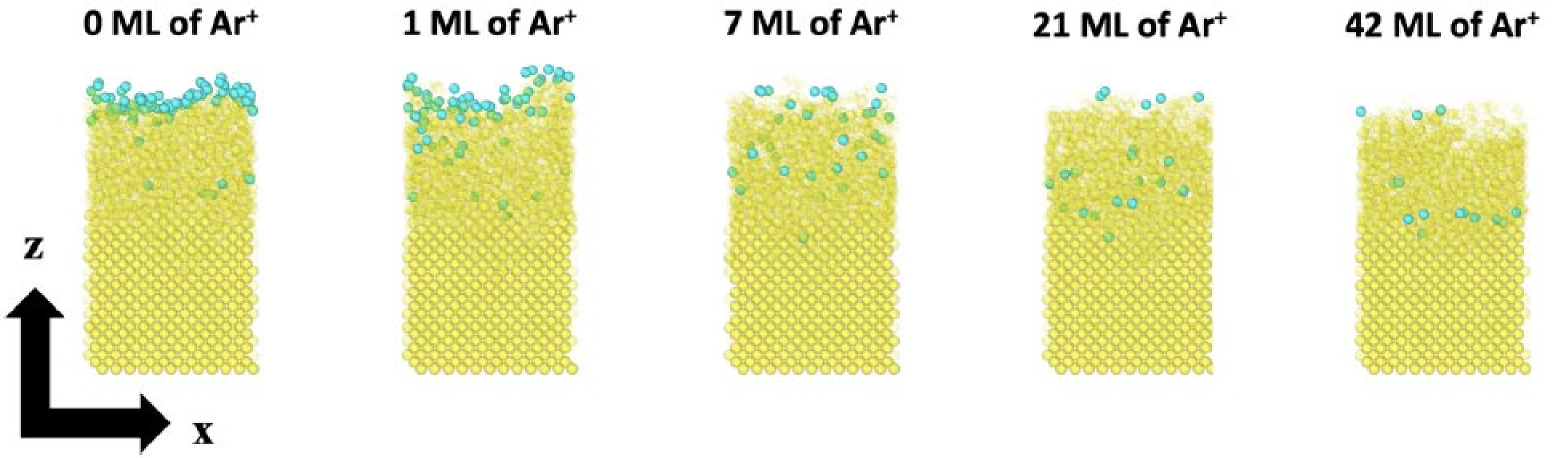

What's Happening Near the Surface?

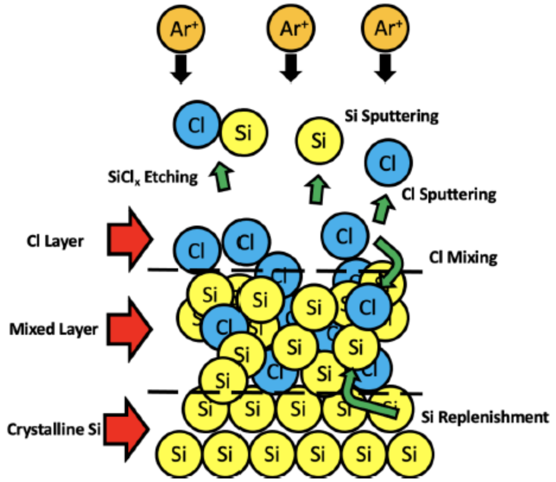

Vella and Graves, J. Vac. Sci. Technol. A 41, 042601 (2023)

Conclusions

The Future of Plasma and Feature Scale Modeling

- Complexity of microelectronics technologies increasing immensely:
  - 3D architectures
  - nm-sized features
  - Atomic level precision during manufacturing on 300 mm wafers
- Precise control of every aspect of the plasma required.
- Resulting complexity making modeling ever more critical for advancing plasma technology.

3D Memory

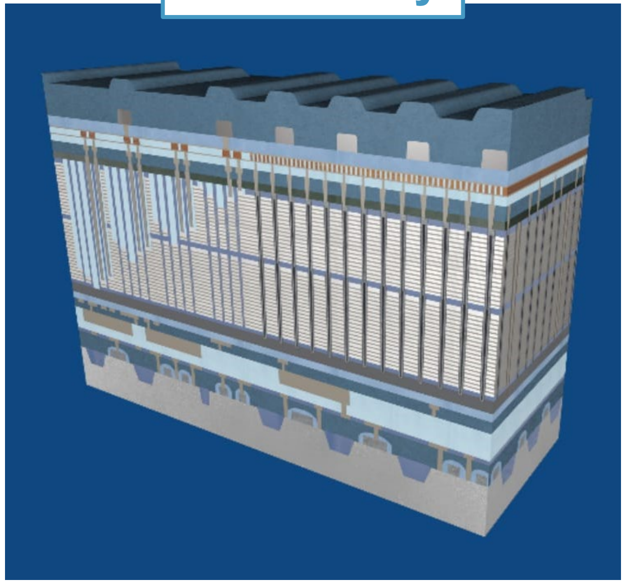

Gate All Around Transistor

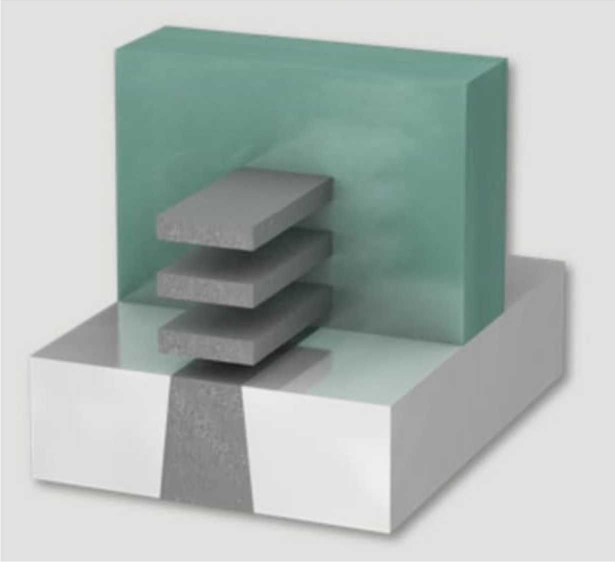

Typical Plasma Etch Process

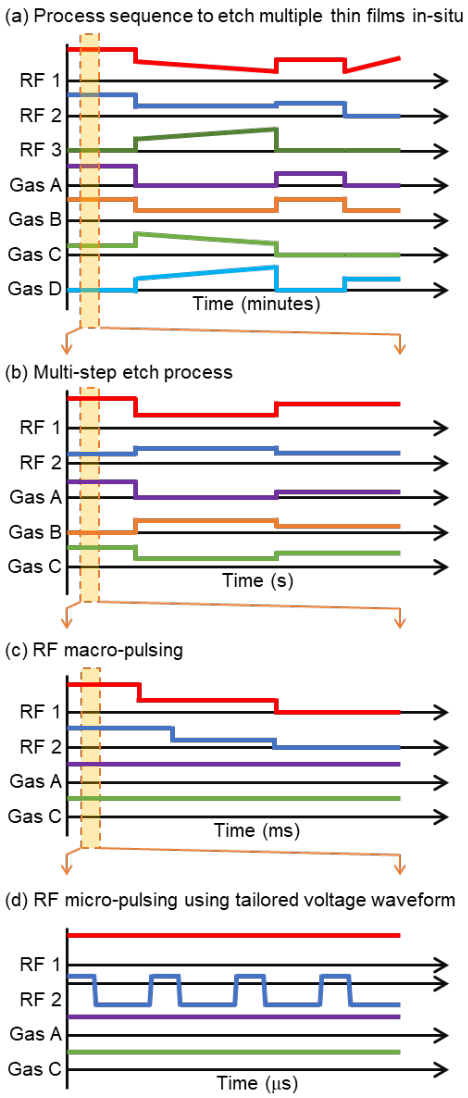

Conclusions

- Low T_e plasmas are a vital technology used for microelectronics manufacturing.
- Plasma modeling plays active role in plasma technology development in industry.
- Semiconductor industry is one of the largest employer of plasma modeling engineers.

- Plasma modeling engineers in industry:
  - Actively participate in R&D, product design, and customer communication
  - Use a variety of specialized software tools
  - Work on a diverse set of technically challenging problems
  - Need strong foundation in plasma physics and plasma – surface interactions to be successful

- Examples were used to illustrate the types of modeling work done in industry.
- Close connection to experiments and focus on solving major technological problems are key.

APPLIED MATERIALS®

make possible